27 April 2026

The Southern Ocean CO2 sink in an evolving observing system

Louise Delaigue[1], Peter Landschützer[2], Cathy Wimart-Rousseau[3], Lisandro Ariel Arbilla[4], Jean-Baptiste Sallée[5], Seth M Bushinsky[6], Hervé Claustre[7], Raphaëlle Sauzède[8]

1. Laboratoire d'Océanographie de Villefranche
2. Flanders Marine Institute
3. National Oceanography Centre
4. Departamento de Ciencias de la Atmósfera y los Océanos, Facultad de Ciencias Exactas y Naturales, Universidad de Buenos Aires (UBA),
5. Sorbonne Université, CNRS/IRD/MNHN, LOCEAN-IPSL, Paris, France
6. University of Hawai'i at Manoa
7. Laboratoire d'Océanographie de Villefranche
8. Institut de la mer de Villefranche

Keywords

carbon sink, southern ocean, autonomous platforms, air-sea CO2 flux, machine learning

Posted on 27 April 2026 — The copyright holder is the author/funder. All rights reserved. No reuse without permission. — This is a preprint and has not been peer reviewed. Data may be preliminary. — https://doi.org/10.22541/essoar.15002449/v1

The Southern Ocean CO_2 sink in an evolving observing system

Louise Delaigue[1], Peter Landschützer[2], Cathy Wimart-Rousseau[3], Lisandro A. Arbilla[4,5,6], Jean-Baptiste Sallée[4], Seth Bushinsky[7], Hervé Claustre[1] and Raphaëlle Sauzède[8]

[1]Sorbonne Université, CNRS, Laboratoire d'Océanographie de Villefranche, Villefranche-Sur-Mer, France
[2]Flanders Marine Institute (VLIZ), Jacobsenstraat 1, 8400 Ostend, Belgium
[3]National Oceanography Centre Southampton, European Way, Southampton, SO14 3ZH, UK
[4]LOCEAN, Sorbonne Université, CNRS, IRD, MNHN, Laboratoire d'Océanographie et du Climat: Expérimentations et Approches Numériques, LOCEAN/IPSL, 75005 Paris, France
[5]Instituto Argentino de Oceanografía (IADO, CONICET-UNS), Bahía Blanca, Argentina
[6]Departamento de Geografía y Turismo, Universidad Nacional del Sur (UNS), Bahía Blanca, Argentina
[7]Department of Oceanography, SOEST, University of Hawai'i at Manoa, Honolulu, HI, USA
[8]Sorbonne Université, CNRS, Institut de la Mer de Villefranche, Villefranche-Sur-Mer, France

Corresponding author: Louise Delaigue (louise.delaigue@imev-mer.fr)

Abstract (250 words max)

The Southern Ocean is a major sink for atmospheric CO_2, yet the magnitude and trend of this sink remain uncertain due to sparse and seasonally biased observations. Reconstructions based on the Surface Ocean CO_2 Atlas (SOCAT) indicate a strengthening of this sink since the early 2000s, but such signals may reflect evolving observational coverage rather than basin-scale change. Here, we combine SOCAT with partial pressure of CO_2 (pCO_2) estimates from BioGeoChemical (BGC-) Argo floats to assess how expanded autonomous sampling alters estimates of Southern Ocean air–sea CO_2 exchange. Using feedforward multilayer perceptron (MLP) models trained on (i) SOCAT-only, (ii) BGC-Argo-only, and (iii) merged, uncertainty-weighted SOCAT + BGC-Argo data, we compute monthly air–sea CO_2 fluxes south of 30°S for 2003-2024. Ship-only observations imply a strong intensification of the CO_2 sink, but this signal disappears once floats are included, yielding a combined reconstruction with a near-zero long-term trend that is not statistically significant. The uncertainty-weighted combined reconstruction yields a mean Southern Ocean CO_2 uptake of -1.32 ± 0.10 Pg C yr^{-1} over this period and is consistent with atmospheric inversion and global ocean biogeochemical model estimates from the Global Carbon Budget. Correcting for sampling biases using BGC-Argo floats reduces the inferred basin-scale sink by 12%, consistent with observing system simulation experiments, while limiting reported systematic biases in float-derived pCO_2 by anchoring autonomous observations to ship-based measurements. Integrating complementary observation streams provides a physically interpretable benchmark for Southern Ocean CO_2 uptake and illustrates how treatment of sampling biases can reconcile ship- and float-derived constraints.

Plain language summary (200 words max)

The Southern Ocean plays a major role in slowing climate change by absorbing large amounts of carbon dioxide (CO_2) from the atmosphere. However, quantifying its total CO_2 uptake and long-term evolution remains challenging because basin-scale estimates rely on sparse, seasonally biased observations, largely from ship-based measurements concentrated in summer and leave substantial gaps in space and time. In this study, we combine ship observations from the Surface Ocean CO_2 Atlas (SOCAT) with year-round measurements from autonomous BioGeoChemical Argo (BGC-Argo) floats, which sample regions and seasons ships rarely reach, especially during winter. Using machine learning methods, we compare CO_2 uptake estimates based on ships alone, floats alone, and both data sources. We find that estimates based only on ship data suggest a strong and increasing CO_2 sink, but this apparent strengthening is reduced by about 12% when float data are included. By correcting for sampling biases and combining both observing systems, we estimate that the Southern Ocean absorbed about 1.32 billion tonnes of carbon per year between 2003 and 2024. This value is consistent with independent estimates from atmospheric data and ocean models and provides a more reliable benchmark for understanding the Southern Ocean's role in the global carbon cycle.

Key points (140 characters max each)

1. Including winter observations from autonomous platforms yields a Southern Ocean CO_2 mean uptake of -1.32 ± 0.10 Pg C yr^{-1} over 2003-2024.
2. Correcting regional and seasonal processes yields a near-zero basin-scale trend despite strengthening inferred in previous studies.
3. Supplementing ship observations with autonomous platforms enables robust detection of future change in Southern Ocean CO_2 uptake.

1 Introduction

The ocean plays a central role in the global carbon cycle by absorbing a substantial fraction of atmospheric carbon dioxide (CO_2; Friedlingstein et al., 2025). Among the global ocean basins, the Southern Ocean is especially important, accounting for an estimated 35-45% of total oceanic carbon uptake despite covering only about one-fifth of the ocean surface area (DeVries & Deutsch, 2014; Gruber et al., 2019). This disproportionate uptake results from a balance set by the Southern Ocean overturning circulation. In the southernmost regions, upwelling of carbon-rich deep waters tends to promote CO_2 outgassing, although the associated supply of nutrients can also support biological drawdown during productive seasons (Hauck et al., 2015; Gray et al., 2018; Bushinsky et al., 2019; Gruber et al., 2019). Further north, strong uptake of anthropogenic CO_2 occurs where mode and intermediate waters form and subduct, transferring carbon into the ocean interior (Sabine et al., 2004; Mikaloff Fletcher et al., 2006; Khatiwala et al., 2013; Gruber et al., 2019).

The persistence of the Southern Ocean CO_2 sink is critical for moderating the rate of atmospheric CO_2 accumulation and associated climate change (Le Quéré et al., 2007; Hauck et al., 2023a; Olivier & Haumann, 2025). Earth system model projections show that even small changes in ocean carbon uptake can significantly affect global temperature trajectories and carbon budget estimates (IPCC, 2023). In high-emissions scenarios, the Southern Ocean is expected to continue absorbing CO_2 in the 21st century, but with considerable uncertainty in its future magnitude due to the limited confidence in its sensitivity to climate feedbacks (Chikamoto & DiNezio, 2021; Mongwe et al., 2024). There is therefore an urgent need for reliable observation-based estimates of the Southern Ocean carbon sink and its historical

variability to evaluate climate models, constrain future projections, and better understand how climate feedbacks shape Southern Ocean carbon uptake.

Despite its critical role in regulating atmospheric CO_2 growth and shaping future climate projections, the magnitude, variability and long-term evolution of Southern Ocean air-sea CO_2 fluxes remain uncertain. Observation-based reconstructions reveal substantial decadal fluctuations, including a weakening in the 1980s–1990s, a reinvigoration after the early 2000s, and a slowdown after 2011, primarily controlled by wind and circulation variability (Le Quéré et al., 2007; Takahashi et al., 2012; Landschützer et al., 2015; Gruber et al., 2019; Keppler & Landschützer, 2019). However, while observation-based reconstructions consistently indicate a strengthening of Southern Ocean CO_2 uptake since the early 2000s, the magnitude of this increase remains poorly constrained, with substantial spread among estimates (Landschützer et al., 2015; Keppler & Landschützer, 2019; Hauck et al., 2023a). Recent estimates place the mean annual CO_2 uptake south of 35°S at approximately -0.95 ± 0.21 Pg C yr^{-1} for the period 2000-2018, with individual methods ranging from -0.71 to -1.25 Pg C yr^{-1} depending on data sources and modelling frameworks (Hauck et al., 2023a). This corresponds to roughly one-third to one-half of the global ocean anthropogenic carbon sink (~2.9 ± 0.4 Pg C yr^{-1} during the decade 2014–2023; Friedlingstein et al., 2025), highlighting both its major contribution to oceanic uptake of anthropogenic CO_2 and the challenge of accurately constraining Southern Ocean variability within the global carbon budget.

The nearly twofold spread in flux estimates stems largely from sparse and uneven observational coverage (Fay et al., 2014; Gray et al., 2018), with surface ocean partial pressure of CO_2 (pCO_2) measurements historically concentrated along ship tracks and heavily biased toward summer months (Bakker et al., 2016). Such under-sampling limits our ability to capture seasonal and regional variability, particularly during winter and in high-latitude sectors poleward of ~50–55°S, leading to substantial uncertainty in flux reconstructions (Rustogi et al., 2023). This challenge is further underscored by recent studies combining satellite-derived surface observations with flux reconstructions that suggest winter CO_2 outgassing south of 50°S has been underestimated by up to 40% due to persistent winter observational gaps, highlighting potential limitations of traditional flux reconstructions based primarily on ship observations and lacking year-round coverage (Zhang et al., 2025).

Reconstruction methods trained on seasonally biased datasets may also amplify spurious trends or variability due to the lack of observational constraints in key regions and seasons (Gloege et al., 2021; Hauck et al., 2023a). Studies using observing system simulation experiments (OSSEs) have shown that reconstructions relying solely on Surface Ocean CO_2 Atlas (SOCAT) data can overestimate decadal trends in surface ocean pCO_2 by more than a factor of two, due to spatial and temporal data gaps (Denvil-Sommer et al., 2021). Recent analysis further demonstrates that air–sea CO_2 flux reconstructions are highly sensitive to the addition of a small number of observations in data-sparse regions. Using successive SOCAT releases, Fay et al. (2025) showed that the inclusion of a limited set of Southern Ocean ship observations reduced global ocean CO_2 uptake estimates by ~0.25–0.30 Pg C yr^{-1}, highlighting how sparse but influential spatio-temporal additions to the Southern Ocean observing network can exert disproportionate influence on basin- and global-scale flux estimates. The issue is not only spatial but also temporal: coarse or infrequent sampling may miss short-lived (i.e., days to months) but significant flux events, further skewing trend estimates (Dong et al., 2024). These challenges highlight the need for a more comprehensive Southern Ocean observing network and evenly distributed observations across the full seasonal and latitudinal spectrum of the Southern Ocean.

One approach to mitigating observational limitations has involved the deployment of autonomous platforms, which offer expanded temporal and spatial resolution. For example, recent studies have shown that even limited additions of surface pCO_2 measurements from racing sailboats or saildrones can significantly alter regional air-sea CO_2 flux estimates, particularly in under-sampled regions of the Southern Ocean (Behncke et al., 2024; Heimdal et al., 2024; Behncke et al., 2026). Similarly, autonomous BioGeoChemical-Argo (BGC-Argo) floats have emerged as a scalable observing system capable of sustained operation across all seasons and regions, providing new constraints on Southern Ocean carbon fluxes and variability (Chai et al., 2020; Claustre et al., 2020). This network can now provide year-round pCO_2 estimates derived from float-based observations of pH, temperature, salinity, and oxygen using neural-network–based carbonate system reconstructions (e.g., CANYON-B and CONTENT; Sauzède et al., 2017; Bittig et al., 2018). Because float observations provide more uniform sampling in space and time, random errors in the underlying float sensor measurements and in the derived pCO_2 estimates tend to average out at basin scale, whereas systematic offsets (e.g., sensor biases or algorithmic biases) persist and must be explicitly constrained (Heimdal & McKinley, 2024). This distinction between random uncertainty and systematic bias is particularly important in data-sparse regions, where even a small number of observations can strongly shape reconstructed fluxes (Fay et al., 2025). However, float-based pCO_2 estimates can still exhibit systematic offsets arising from uncertainties in carbonate system constants, sensor calibration and pH adjustment procedures, and the estimation of alkalinity used in carbonate-system reconstructions. Biases may also arise from small offsets in float oxygen sensors that propagate into derived carbonate system variables and air–sea CO_2 flux estimates if left uncorrected (Bushinsky et al., 2025). Unlike ship-based observations, however, float sampling is not strongly concentrated in specific regions or seasons and therefore does not introduce comparable systematic sampling biases (Bittig et al., 2019).

Enhanced float-based observational coverage has led to several important insights (Heimdal & McKinley, 2024). For instance, floats have revealed widespread wintertime CO_2 outgassing south of the Polar Front (48–60°S), indicating that earlier basin-scale flux estimates based primarily on ship data may have overstated net annual uptake (Gray et al., 2018; Bushinsky et al., 2019). Although ship-based observations can capture winter outgassing in some well-sampled regions, such as the Drake Passage, their limited temporal presence across most of the Southern Ocean has hindered the resolution of the full seasonal cycle at basin scale (Gray et al., 2018; Bushinsky et al., 2019). Combining float-based pCO_2 estimates with traditional ship-based measurements has also been shown to significantly lower estimates of Southern Ocean CO_2 uptake estimate by as much as 0.4 Pg C yr^{-1} by reducing sampling biases (Bushinsky et al., 2019; Bushinsky et al., 2025). More broadly, this expanded observational network has improved agreement between observation-based flux products and ocean biogeochemical models, which tend to simulate a more moderate and stable Southern Ocean sink over recent decades than suggested by ship-only reconstructions (Bushinsky et al., 2019; Heimdal & McKinley, 2024).

Many early studies incorporating float observations focused on short time periods (often <5 years) and primarily relied on high-latitude floats from a single program (SOCCOM), largely concentrated south of ~50–55°S, limiting their ability to resolve long-term trends or assess mid-latitude regions north of the Polar Front (~35–50°S) that account for a substantial share of the net flux (Bushinsky et al., 2019; Hauck et al., 2023b). Moreover, important methodological differences in float-based pCO_2 estimation and model–data comparison frameworks complicate cross-study interpretation. These include differences in how float pCO_2 is derived from carbonate-system proxies (e.g., approaches based on pH with estimated alkalinity versus more empirical multivariable reconstructions), how systematic biases are corrected, and how float observations are integrated or compared with mapping products and models (Watson et al., 2020; Mackay et al., 2022). As a result, cross-study comparisons of Southern Ocean CO_2

flux magnitude and trends remain difficult. More fundamentally, key questions remain about the intensity and temporal evolution of the Southern Ocean carbon sink, specifically, whether the observed strengthening in recent decades reflects a robust signal or is influenced by evolving observational coverage.

Here, we aim to constrain the magnitude and temporal evolution of the Southern Ocean CO_2 sink over the past two decades by explicitly accounting for the evolving observational coverage provided by ship- and float-based measurements. By comparing flux reconstructions produced by MLP models trained on different observing-system configurations, we isolate the influence of sampling and distinguish variability driven by observational coverage from that reflecting underlying carbon-cycle processes. Specifically, we quantify the Southern Ocean carbon sink under conditions of maximal spatiotemporal coverage, using the full extent of available BGC-Argo float data south of 30°S. We combine the most recent release of the SOCAT (SOCAT; Bakker et al., 2016) with pCO_2 estimates derived from BGC-Argo floats, and train a suite of machine-learning reconstructions using a multilayer perceptron (MLP): (i) SOCAT-only, (ii) float-only, and (iii) a combined SOCAT and float reconstruction in which observations are weighted by their associated uncertainties during model training. We then assess the consistency of our estimate with independent constraints from atmospheric inversions, ocean biogeochemical models, and observation-based fCO_2 products synthesized in the Global Carbon Budget. By explicitly accounting for sampling geometry and platform-specific uncertainties, this framework clarifies how apparent discrepancies among observing systems arise and provides a robust, observation-based benchmark for Southern Ocean CO_2 uptake under an evolving observing system.

2 Methods

2.1 SOCATv2025

Version 2025 of the Surface Ocean CO_2 Atlas (SOCATv2025) was used as the primary source of surface ocean fugacity of CO_2 (fCO_2) measurements. This release includes data through the end of 2024. SOCAT is a globally compiled, quality-controlled dataset that integrates underway fCO_2 observations from research vessels and moored platforms, following standardized data processing protocols and quality assurance procedures (Figs. 1; Bakker et al., 2016). Each measurement is assigned a quality flag reflecting data accuracy and processing level, with the highest-quality SOCAT flags typically associated with an uncertainty of approximately ±2–5 µatm in surface fCO_2 (Bakker et al., 2016). In this study, we adopt a conservative uncertainty of 5 µatm for all SOCAT observations, as we use the gridded SOCAT product and cannot distinguish between individual quality flags within each grid cell.

2.2 BGC-Argo float array

To supplement ship-based surface observations, data from the global network of biogeochemical (BGC) Argo profiling floats were included. These autonomous floats typically profile the upper 2,000 meters of the ocean every 10 days and are equipped with a core suite of sensors, including temperature, salinity, and dissolved oxygen (Fig. 1; Johnson & Claustre, 2016; Roemmich et al., 2019; Claustre et al., 2020).

Float-based carbonate system estimates were obtained from a monthly global BGC-Argo product distributed by the Copernicus Marine Service (Copernicus product ID: MULTIOBS_GLO_BGC_NUTRIENTS_CARBON_PROFILES_MYNRT_015_009). This product is generated by applying the CANYON-B (Carbonate system and Nutrients concentration from hYdrological properties and Oxygen using a Neural-network) and CONTENT (Carbonate system from

Neural-neTwork) neural network algorithms, trained on the GLODAPv2 reference dataset (Global Ocean Data Analysis Project version 2; Olsen et al., 2016; Lauvset et al., 2021), to float-measured pressure, temperature, salinity, oxygen, location, and date in order to estimate total alkalinity (TA), dissolved inorganic carbon (DIC), pH, and pCO_2 (Sauzède et al., 2017; Bittig et al., 2018).

Unlike approaches that derive pCO_2 from float pH measurements combined with estimated alkalinity, the Copernicus product used here infers carbonate system variables from neural-network relationships constrained by float-measured temperature, salinity, oxygen, and hydrographic context (CANYON-B/CONTENT; Sauzède et al., 2017; Bittig et al., 2018). In this framework, pCO_2 is not directly constrained by discrete pCO_2 observations but is calculated during training from GLODAPv2 total alkalinity and dissolved inorganic carbon using standard carbonate system thermodynamics (Sauzède et al., 2017; Bittig et al., 2018). The neural networks therefore learn empirical relationships linking hydrographic and oxygen variability to carbonate system properties represented in the GLODAP reference dataset. To account for long-term anthropogenic carbon increases, decimal year is included as an input variable during training, allowing reconstructed carbonate system fields to evolve temporally rather than representing a static climatology (Bittig et al., 2018). Previous evaluations indicate that these mappings reproduce large-scale spatial and temporal variability in surface pCO_2 with no significant global mean bias, although uncertainties increase in regions where oxygen and carbon cycles are weakly coupled, particularly in highly productive surface waters (Bittig et al., 2018). Because carbonate system variables are inferred from multivariate relationships rather than calculated directly from float pH and estimated alkalinity, this framework also avoids the explicit propagation of uncertainties associated with pH-based pCO_2 reconstructions.

Recent work has identified a systematic negative bias in oxygen measurements from air-calibrated BGC-Argo floats relative to shipboard reference profiles, which propagates into carbonate system variables estimated from these data. Specifically, float oxygen offsets of approximately -2.7 µmol kg^{-1} at depth lead to an overestimation of surface pCO_2 by +3.2 µatm when using neural network algorithms (Bushinsky et al., 2025). While this oxygen bias is well-documented at depth, no comprehensive study to date has quantified the equivalent bias in surface waters. Nevertheless, we apply a uniform -3.2 µatm correction to all float-derived surface pCO_2 values prior to training and evaluation of the MLP model, treating it as a conservative lower-bound estimate of the surface bias. This approach improves consistency with ship-based observations and mitigates the influence of known sensor biases on derived air-sea CO_2 flux estimates.

Finally, for each BGC-Argo profile south of 30°S, surface pCO_2 was defined as the mean of observations within the upper 0–10 m. This depth range was chosen because not all floats sample within the first few meters, whereas averaging over 0–10 m provides a more consistent and representative near-surface estimate. While this differs slightly from the 5 m nominal reference depth typically used for SOCAT (see Section 2.1; Bakker et al., 2016), the approach ensures robust coverage across the float array and minimizes sampling gaps in the surface layer. Only profiles for which temperature, salinity, and dissolved oxygen were available in delayed mode, as indicated in the Copernicus index file at the platform and cycle level, were retained to ensure that neural-network-derived carbonate system estimates were based on fully quality-controlled hydrographic and oxygen measurements.

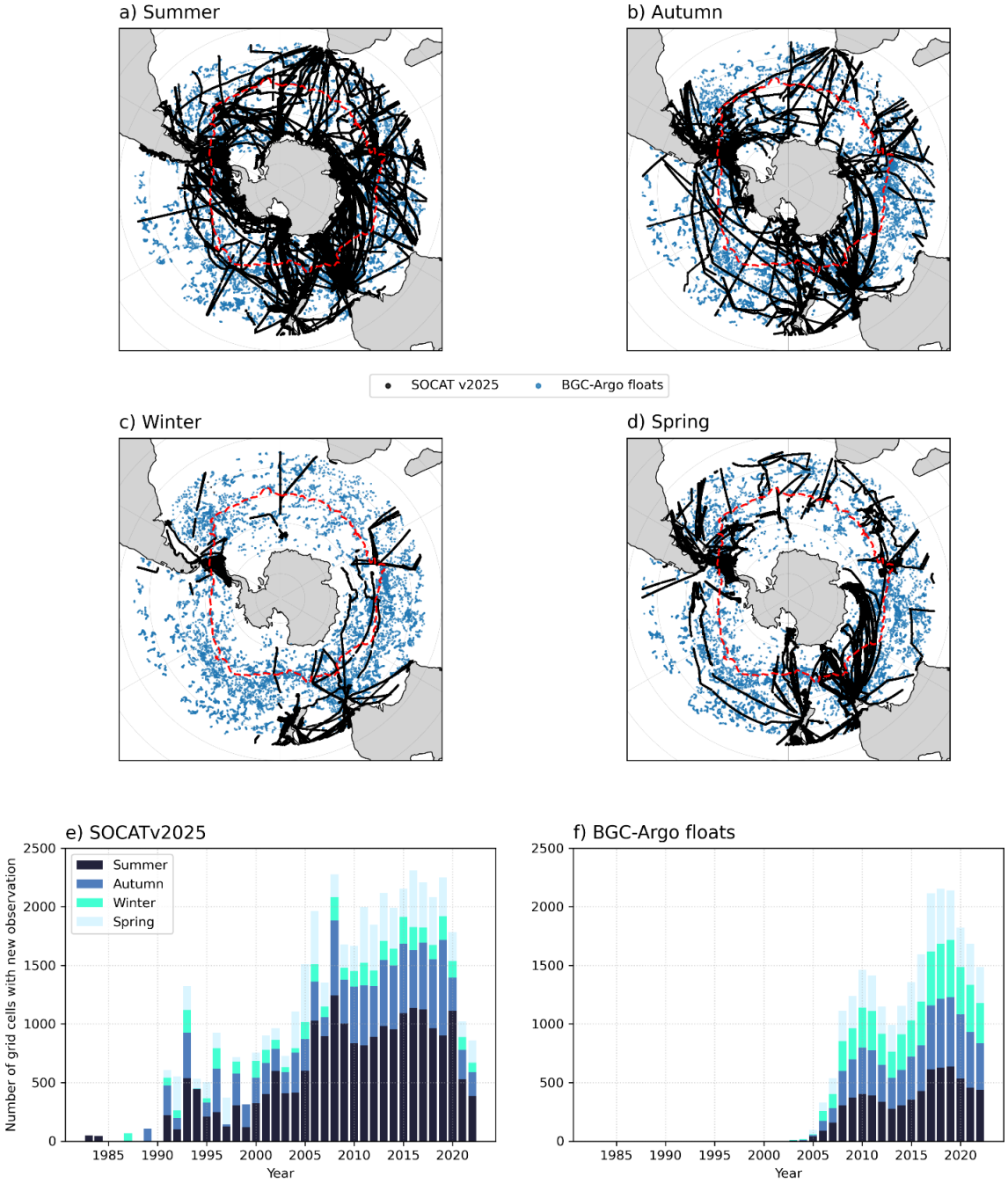


Figure 1. Spatial distribution of surface ocean pCO_2 observations south of 30°S during austral (a) summer, (b) autumn, (c) winter and (d) spring. Black dots represent SOCATv2025 observations from 1983 to 2024, while blue dots show BGC-Argo float observations from 2003 to 2025. The dashed red line indicates the climatological position of the Polar Front (Park and Durand, 2019; Park et al., 2019). (e–f) Annual count of 1° × 1° grid cells south of 30°S containing at least one new observation in each year, shown as seasonal stacked bars for (e) SOCATv2025 and (f) BGC-Argo. Seasons are defined climatologically: Summer (Dec-Feb), Autumn (Mar-May), Winter (Jun-Aug), and Spring (Sep-Nov).

2.3 Multilayer perceptron model

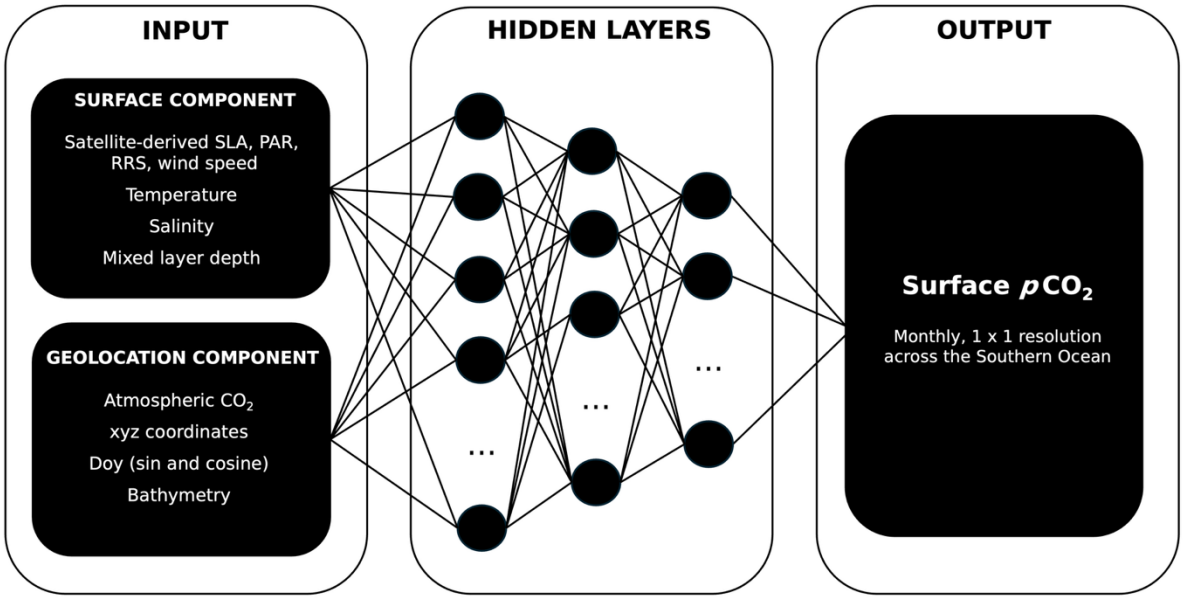


Figure 2. Schematic of the multi-layer perceptron (MLP) used to estimate surface ocean partial pressure of CO_2 (pCO_2) in the Southern Ocean. Input features are grouped into two components: surface (satellite-derived sea level anomaly (SLA), Photosynthetically active radiation (PAR), remote sensing reflectance (RRS), wind speed, temperature, salinity and mixed layer depth) and geolocation (atmospheric CO_2, spatial coordinates, seasonal cycle encoded as sine and cosine of day of year, bathymetry). These inputs are processed through three hidden layers to produce monthly pCO_2 estimates at 1° × 1° spatial resolution across the Southern Ocean.

We use a feedforward multilayer perceptron (MLP) model trained to predict surface ocean pCO_2 following the Satellite Ocean-Color merged with Argo (SOCA) methodology originally introduced by Sauzède et al. (2016) and later adapted in Renosh et al. (2023). The SOCA framework integrates satellite-derived surface observations with *in-situ* vertical profiles to train neural networks that estimate the vertical distribution of several biogeochemical properties (i.e., the suspended particles, the chlorophyll-a concentration and the light availability). While earlier SOCA models focused on subsurface properties, the present implementation applies the same core principles to surface ocean pCO_2. Using the collocated satellite and in situ matchups described in Sections 2.3.1-2.3.7, the model leverages an ensemble of neural networks to capture the spatial and temporal variability of surface pCO_2 across the Southern Ocean. Throughout this manuscript, "MLP model" refers to the trained neural network, while "reconstruction" refers to the spatially and temporally complete pCO_2 field produced by applying that model to the full predictor dataset.

2.3.1 Predictive variables

Full details of data sources, preprocessing, and spatial–temporal harmonization are provided in Text S1 of the Supplementary Material. Briefly, predictor variables were selected to represent physical circulation, biological activity, and atmospheric forcing known to influence surface ocean pCO_2. These included surface temperature, surface salinity, mixed layer depth (MLD), sea level anomaly (SLA), photosynthetically available radiation (PAR), remote sensing reflectance (RRS), wind speed,

atmospheric pCO_2. All variables were harmonized onto a common monthly 1° × 1° grid south of 30°S for the 2003–2024 analysis period.

Temperature, salinity and MLD were obtained from the ARMOR3D reanalysis product (Copernicus product ID: MULTIOBS_GLO_PHY_TSUV_3D_MYNRT_015_012). SLA was obtained from the Copernicus Marine Service DUACS multi-satellite altimetry product (Copernicus product ID: SEALEVEL_GLO_PHY_L4_MY_008_047). Ocean-colour products (PAR and RRS; Copernicus product ID: OCEANCOLOUR_GLO_BGC_L3_NRT_009_101; PAR accessed from https://hermes.acri.fr/, last accessed in November 2025) were derived from merged multi-sensor satellite datasets and aggregated to monthly 1° resolution. Wind speed was calculated from ERA5 10-meter zonal (u_{10}) and meridional (v_{10}) wind components. Atmospheric CO_2 was prescribed from the Cape Grim baseline station, representative of well-mixed Southern Ocean air masses (https://capegrim.csiro.au; last accessed in November 2025).

In addition to environmental predictors, derived spatiotemporal features were included to represent structured variability in space and time. These comprised a cyclical encoding of seasonality, three-dimensional Cartesian coordinates derived from latitude and longitude, and seafloor depth from the GEBCO bathymetry dataset (version 2024; https://www.gebco.net/; last accessed in July 2025).

Together, these predictors capture key drivers of surface pCO_2 variability in the Southern Ocean including circulation and frontal dynamics, biological production, air–sea gas exchange, long-term atmospheric forcing, and spatial–temporal structure.

2.3.2 Data colocation and gridding

All observations and predictor variables were collocated onto a common 1° × 1° monthly grid (2003–2024). Native-resolution fields were aggregated to this grid using median values within each cell–month. Surface pCO_2 observations from SOCAT and BGC-Argo floats were assigned to their corresponding grid cell and month, with medians computed where multiple observations coincided. Only cell–months for which both surface pCO_2 and all predictor variables were available were retained for model training.

This procedure yielded a fully collocated dataset in which each grid cell and month contains a surface pCO_2 value together with the complete set of environmental and spatiotemporal predictors. Expressing all data on a common grid ensured consistent treatment of SOCAT and float observations and prevented regions with dense sampling from disproportionately influencing the model.

For experiments combining SOCAT and float data, the two sources were processed independently through this gridding procedure and subsequently merged.

2.3.3 Data partitioning strategy

To preserve the spatial and temporal structure of observations during model development, the gridded datasets were partitioned into training (70%), validation (15%), and test (15%) subsets using a cluster-aware stratified sampling approach. Spatial and temporal coordinates (longitude, latitude, decimal year, day of year, and elapsed time) were standardized and used as inputs to the HDBSCAN density-based clustering algorithm, which identifies coherent spatiotemporal groupings without requiring a predefined number of clusters. Data splits were then performed within these groupings to ensure that all subsets remained representative of the full range of sampling regimes across the Southern Ocean.

Independent validation cruises were excluded prior to partitioning and retained exclusively for external model evaluation. For experiments combining SOCAT and BGC-Argo data, training, validation, and test subsets were generated separately for each dataset and merged afterward to preserve their internal structure while ensuring balanced representation.

2.3.4 Model training

MLP models were trained separately using SOCAT-only ($MODEL_{SOCAT}$), float-only ($MODEL_{BGC\text{-}Argo\ floats}$), and combined SOCAT–float datasets ($MODEL_{SOCAT\ +\ BGC\text{-}Argo\ floats\ (weighted)}$). All models were trained using standardized predictor variables and early stopping based on validation performance to prevent overfitting.

Training periods differed between datasets: SOCAT-based models were trained using observations from 1997–2024, whereas float-based models were trained over 2003–2024, reflecting the shorter temporal coverage of the BGC-Argo record. Although subsequent flux analyses focus on the common 2003–2024 period, the full SOCAT time series was retained during training to ensure that long-term trends and low-frequency variability were adequately represented in SOCAT-constrained reconstructions.

Because differences in sampling density, uncertainty structure, and seasonal coverage between SOCAT and float-derived pCO_2 require distinct training configurations, model hyperparameters were optimized independently for each dataset rather than enforcing a single uniform architecture across all experiments (see Table S1 of the Supplementary Material). This reflects the primary objective of this study, which is to assess how observational constraints influence reconstructed Southern Ocean carbon fluxes rather than to benchmark neural-network performance. All models were nevertheless trained within a consistent methodological framework and evaluated using identical post-hoc metrics — root mean square error (RMSE) and the coefficient of determination (R^2) — computed on independent held-out validation and test sets, irrespective of the training loss function used. Differences in reconstructed pCO_2 fields therefore reflect observational constraints rather than arbitrary modelling choices.

To account for sensitivity to network architecture and stochastic optimization, an ensemble approach was adopted. Hidden-layer widths were sampled using a fixed random seed within constrained ranges identified from a preliminary broad search (SOCAT-only and float-only experiments: layer 1: 75–90, layer 2: 65–80, layer 3: 60–75 neurons; combined SOCAT–float experiment: layer 1: 90–120, layer 2: 70–100, layer 3: 50–80 neurons, reflecting the increased size and heterogeneity of the merged training set), subject to a monotonic decreasing-width constraint across layers. For each dataset configuration, a random search of over 200 candidate three-hidden-layer MLP architectures was performed and ranked using RMSE. Validation RMSE was used as the sole ranking metric because the primary objective of the reconstruction is accurate prediction of continuous surface pCO_2 fields and derived air–sea CO_2 fluxes; minimizing absolute prediction error is therefore most directly relevant. The ten best-performing architectures were retained to form the structural ensemble used for prediction.

For experiments using the combined SOCAT–float dataset, the model was trained on the mixed observational pool but early stopping and model ranking were both evaluated against the SOCAT-only validation and test subsets. This ensures that selected models are optimised against ship-based observations, which serve as the primary accuracy benchmark, rather than against float-derived targets that may carry their own retrieval uncertainty.

For grid cells and months where both SOCAT and float observations were available, target pCO_2 values were first combined using an inverse-variance weighted mean based on their respective observational uncertainties. The corresponding fused uncertainty was computed from the combined variance of the two sources. During model training, samples were then assigned weights derived from these uncertainties using a bounded transformation $w = 1/(1 + \sigma/\sigma_0)\ with\ \sigma_0 = 5\ \mu atm$ ensuring that observations with larger uncertainties contributed less strongly to parameter updates while avoiding excessively large weights for low-uncertainty samples. In the remainder of this study, we refer to this scheme as *uncertainty-weighted* training, meaning that each training sample contributes to the loss function according to a weight derived from its estimated observational uncertainty. This approach allows heterogeneous target errors across SOCAT and float observations to be accounted for during training while maintaining SOCAT-only metrics for model selection.

Full details of network architecture ranges, optimization settings, training hyperparameters, and ensemble configuration are provided in Table S1 of the Supplementary Material. Model skill was also evaluated using fully independent validation datasets withheld entirely from model development; details of this external validation and associated results are provided in Text S2 and Figures S1–S10 of the Supplementary Material.

2.3.5 Propagation of pCO_2 uncertainty in model training

Uncertainty associated with errors in the pCO_2 training targets was propagated through the reconstruction using a Monte Carlo ensemble approach. This framework quantifies how observational uncertainty in surface pCO_2 influences the reconstructed fields and derived air–sea CO_2 fluxes.

For each dataset configuration, the ten best-performing MLP architectures identified during model training (Section 2.3.4) were used as the structural basis for uncertainty propagation. For each architecture, 100 independent Monte Carlo retrainings were performed in which Gaussian noise was added to pCO_2 values in both the training and validation subsets prior to model fitting. This procedure generated an ensemble of models sampling the range of plausible reconstructions given observational uncertainty.

Perturbations applied to float-derived pCO_2 were sampled using the reported per-sample uncertainty from the BGC-Argo product (Copernicus product ID: MULTIOBS_GLO_BGC_NUTRIENTS_CARBON_PROFILES_MYNRT_015_009). For SOCAT observations, Gaussian perturbations with a standard deviation of 5 µatm were applied as a conservative representation of ship-based measurement uncertainty, consistent with reported accuracy limits for surface pCO_2 observations (Bakker et al., 2016).

Each perturbed dataset was used to retrain the corresponding MLP using identical training configurations to those described in Section 2.3.4. Early stopping and model selection were performed against perturbed validation data to ensure consistency with the assumed observational uncertainty. Across all architectures and perturbation realizations, this procedure yielded 1000 trained models per dataset configuration (10 architectures × 100 perturbations).

Final pCO_2 predictions and associated uncertainties were derived from the distribution of outputs across this Monte Carlo ensemble. The ensemble mean provides the best estimate of surface pCO_2, while the ensemble standard deviation quantifies uncertainty arising from both observational error in the training data and sensitivity of the neural-network reconstruction to those errors. This approach captures

complementary sources of uncertainty associated with model structure, stochastic training, and pCO_2 target uncertainty.

Independent evaluation using withheld SOCAT cruises and BGC-Argo floats is described in the Supplementary Material (see Text S2; see Figs. S1-S10).

2.3.6 pCO_2 predictions

Final surface-ocean pCO_2 fields were generated using the full Monte Carlo ensemble described in Section 2.3.5. For each dataset configuration, predictions were produced using all ensemble members (10 architectures × 100 Monte Carlo realizations; 1000 models total).

Each ensemble member was applied independently to the full predictor dataset to generate monthly 1° × 1° surface pCO_2 fields across the Southern Ocean. The final pCO_2 estimate at each grid cell and month was computed as the ensemble mean across all model realizations, while reconstruction uncertainty was quantified as the ensemble standard deviation.

This ensemble-based framework yields spatially and temporally continuous estimates of Southern Ocean surface pCO_2 together with uncertainty fields that reflect propagated observational error, model structural variability, and stochastic training effects. Seasonal distributions of prediction uncertainty and example reconstructed fields are provided in the Supplementary Material (Figs. S9–S14).

2.3.7 Spatiotemporal coverage

To assess the extent to which surface ocean pCO_2 is sampled or predicted across space and time, we computed the spatiotemporal coverage of each dataset (SOCAT, BGC-Argo floats, their combination, and the MLP model ensemble) over the common period from January 2003 to December 2024. Coverage was evaluated using a 1° × 1° grid south of 30°S, with monthly temporal resolution, resulting in 264 potential time steps per grid. A spatiotemporal bin was considered filled if at least one observation (or prediction, in the case of the model matrix) was available within the corresponding grid cell during a given month. We computed the percentage of bins filled for each dataset relative to this total (Table 1).

To evaluate seasonal coverage, we assigned each observation to one of four climatological seasons (Summer: December-February; Autumn: March-May; Winter: June-August; Spring: September-November). A grid cell was considered covered for a given season each year if it contained at least one observation in any of the three months comprising that season. Seasonal coverage was then expressed as the percentage of these bins that were filled (Table 1).

To visualize the spatial completeness of model predictions, we also mapped the percentage of the study period (2003-2024) for which each grid cell contained at least one pCO_2 prediction from the MLP ensemble (Fig. 3).

450

Dataset	Total	Summer	Autumn	Winter	Spring
OBS_{SOCAT}	1.2%	5.7%	3.0%	1.0%	2.2%
$OBS_{BGC\text{-}Argo\ floats}$	0.7%	2.4%	1.9%	1.1%	1.9%
$OBS_{SOCAT\ +\ BGC\text{-}Argo\ floats}$	1.9%	8.0%	4.8%	2.1%	3.9%
$MODEL_{SOCAT\ +\ BGC\text{-}Argo\ floats}$	67.9%	89.9%	87.9%	60.5%	74.3%
Increase of model vs. obs.	+65.9%	+81.7%	+82.9%	+58.2%	+70.2%

451 **Table 1.** Spatiotemporal coverage (%) by data source and season over the common period 2003–2024.
452 Monthly coverage represents the percentage of filled (year, month, latitude, longitude) bins across 264
453 months, where a bin is considered filled if it contains at least one value during that month. Seasonal
454 coverage represents the percentage of ocean grid cells that contain at least one observation within any
455 month of a given season, for each year, expressed over the fixed denominator of all ocean grid cells
456 multiplied by the number of years (22). The final row reports the absolute percentage-point increase in
457 coverage provided by $MODEL_{SOCAT\ +\ BGC\text{-}Argo\ floats}$ relative to $OBS_{SOCAT\ +\ BGC\text{-}Argo\ floats}$.

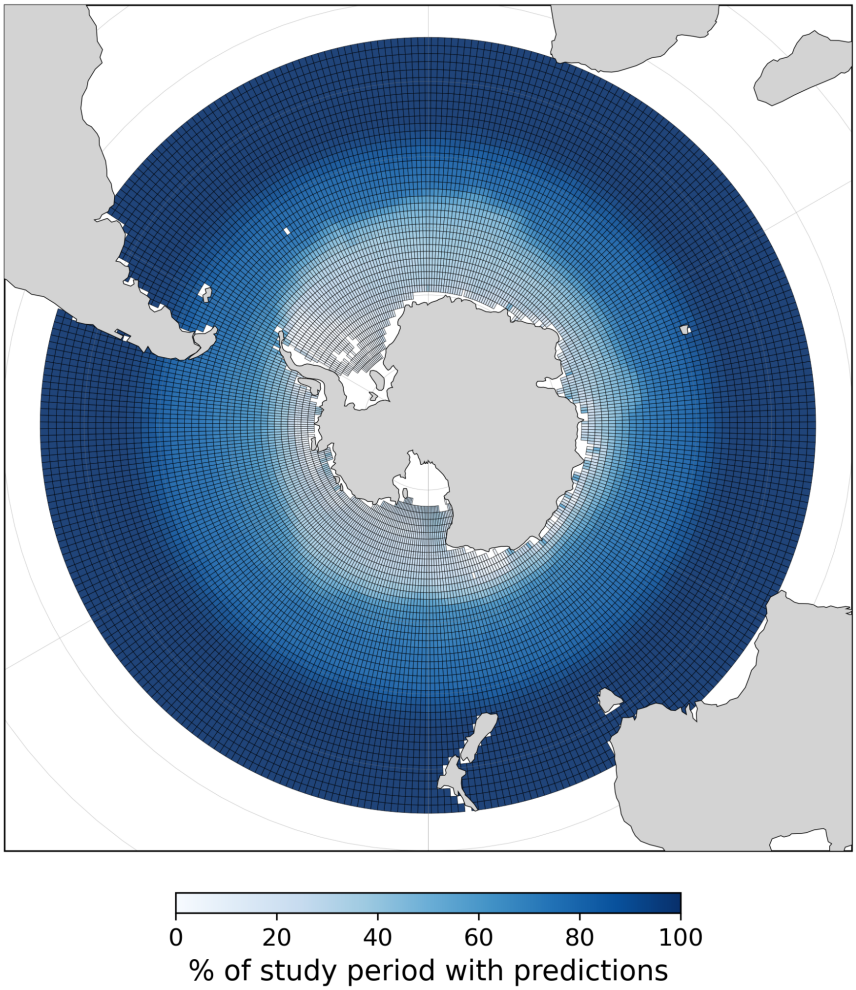


Figure 3. Percentage of the study period (2003-2024) with pCO_2 predictions from the MLP ensemble in each 1° × 1° grid cell south of 30°S. Coverage is expressed as the fraction of months for which predictions are available per grid cell over the study period.

2.4 Air-sea CO_2 fluxes

2.4.1 Flux calculation

A continuous, gap-filled monthly matrix of surface ocean pCO_2 for the Southern Ocean was generated on a 1° × 1° spatial grid for the period 2003-2024 using the ensemble predictions described above. The same flux calculation was applied both to the machine-learning reconstructions and to observation-based pCO_2 fields derived directly from SOCAT, BGC-Argo floats, and their combined dataset to generate the observation-only flux time series used for comparison. Subsequently, observation-based flux estimates derived directly from uninterpolated data are labelled OBS (i.e., OBS_{SOCAT}, $OBS_{BGC\text{-}Argo\ floats}$ and $OBS_{SOCAT+BGC\text{-}Argo\ floats}$), while flux estimates derived from the corresponding MLP reconstructions are labelled MODEL (i.e., $MODEL_{SOCAT}$, $MODEL_{BGC\text{-}Argo\ floats}$ and $MODEL_{SOCAT+BGC\text{-}Argo\ floats\ (weighted)}$).

This gridded pCO_2 product enables the estimation of air-sea CO_2 fluxes across the Southern Ocean. Air-sea CO_2 fluxes were calculated using the standard bulk formulation (Wanninkhof, 1992; Ho et al., 2006; Wanninkhof, 2014):

$$F = k \times K_0 \times (pCO2_{sea} - pCO2_{air}) \quad (1)$$

where F denotes the net flux of CO_2 across the ocean-atmosphere boundary, k is the gas transfer coefficient, K_0 is the temperature- and salinity-dependent solubility of CO_2 in seawater, and $pCO2_{sea} - pCO2_{air}$ represents the air-sea pCO_2 gradient. Positive flux values indicate net CO_2 release from the ocean to the atmosphere (outgassing), while negative values reflect oceanic CO_2 uptake. Gas-transfer velocity was estimated using the parameterization of Ho et al. (2006), and flux calculations were performed using the *pySeaFlux* software package (version 2.2.2; Fay et al., 2021).

Monthly flux densities were computed on the 1° × 1° grid using reconstructed surface pCO_2 together with colocated temperature, salinity, wind speed, and atmospheric CO_2 fields. Fluxes were converted from mol C m^{-2} d^{-1} to monthly carbon fluxes using the number of days per month and then area-weighted using grid-cell surface area. Basin-integrated air–sea CO_2 fluxes south of 30°S were obtained by first computing an area-weighted mean flux density across the 1° × 1° grid using latitude-dependent grid-cell surface areas. This basin-mean flux density was then scaled by the total ocean area south of 30°S derived from the GOAS v1 global ocean polygon dataset (Flanders Marine Institute, 2021). Results are reported in Pg C yr^{-1}.

Monthly basin-integrated fluxes were aggregated to annual means. Mean Southern Ocean CO_2 uptake was quantified as the average of annual basin-integrated fluxes over the common analysis period (2003–2024). Linear trends in annual fluxes over 2003–2024 were estimated using ordinary least-squares regression and are reported together with the associated standard error and p-value.

For intercomparison, the same domain-integrated annual means and trend calculations were applied to benchmark products, including Global Carbon Budget surface-ocean pCO_2 products, global ocean biogeochemical models (GOBMs), and atmospheric inversion estimates, after extracting the region south of 30°S (Friedlingstein et al., 2025).

Trends were additionally computed for 2003–2012, 2003–2018 (i.e. for direct comparison to Hauck et al., 2023a), and 2015–2024 and reported as flux trends in Pg C yr^{-1} $decade^{-1}$, with negative values indicating increasing uptake.

2.4.2 Flux uncertainty and statistical significance

Uncertainty in basin-integrated fluxes was estimated by propagating both observational and model-related uncertainties through the flux calculations. Observational uncertainty was represented using reported pCO_2 uncertainties for float-derived values and a conservative ±5 µatm uncertainty for SOCAT-based measurements (Bakker et al., 2016). Model uncertainty was represented by the spread of the Monte Carlo ensemble predictions. Upper and lower flux estimates were computed by perturbing surface pCO_2 fields according to these uncertainties and recomputing fluxes, yielding annual uncertainty estimates that reflect the combined effects of observational and reconstruction errors.

Uncertainty reported alongside mean fluxes (mean ± σ) represents the propagated uncertainty of the 2003–2024 mean rather than the typical uncertainty associated with individual annual flux estimates. To quantify this uncertainty and assess whether mean Southern Ocean CO_2 fluxes were statistically distinguishable from zero, annual basin-integrated fluxes were sampled using a Monte Carlo framework in which each year was represented by a Gaussian distribution defined by the annual mean and its

516 propagated 1σ uncertainty. A total of 200,000 realizations of the 2003–2024 mean flux were generated
517 for each dataset. The standard deviation of the resulting distribution was taken as the uncertainty of the
518 mean, and corresponding 95 % confidence intervals were derived from the same distribution.

519 A mean was considered statistically distinguishable from zero when the associated 95 % confidence
520 interval excluded zero. This procedure was applied consistently to all observation-based,
521 reconstruction-based, and benchmark flux estimates. For all datasets considered here, the 95 %
522 confidence intervals of the mean flux exclude zero, indicating a statistically significant net Southern
523 Ocean CO_2 sink over 2003–2024 across all observational and reconstruction-based estimates (Table S2
524 of the Supplementary Material).

3. Results and Discussion

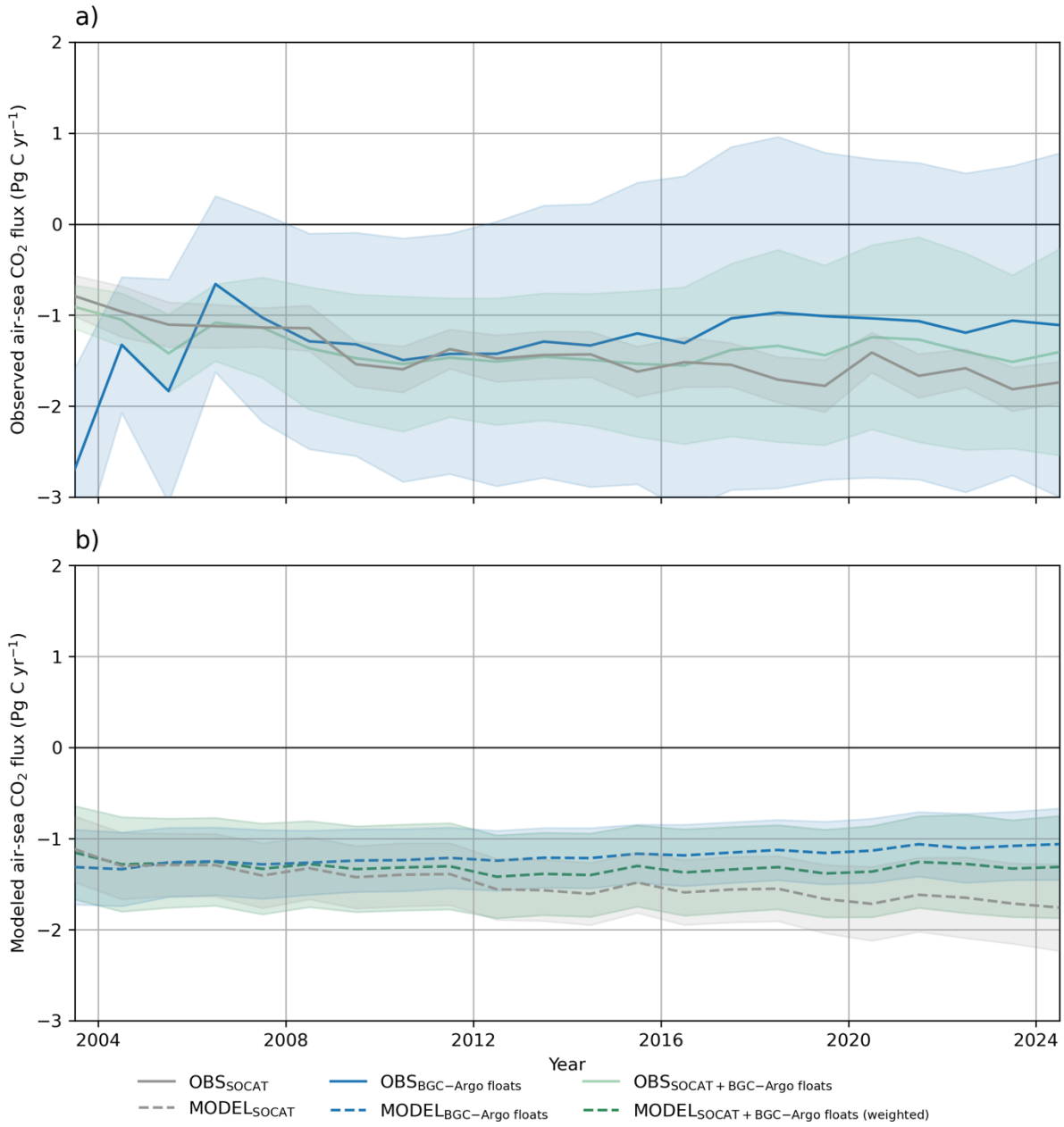


Figure 4. Southern Ocean CO_2 flux estimates were calculated south of 30°S for the period 2003–2024, corresponding to the temporal overlap between SOCAT observations and BGC-Argo float coverage. Fluxes are computed from observational and reconstructed surface pCO_2 fields using the same bulk air–sea CO_2 flux formulation described in Section 2.4.1. (a) Observed annual mean air–sea CO_2 fluxes derived from SOCAT (grey), BGC-Argo floats (blue), and their combined estimate (green). (b) Corresponding reconstruction–based CO_2 flux estimates trained on the observational datasets shown in panel (a), using the same colour coding. Shaded envelopes indicate ±1σ uncertainty on each annual flux estimate derived from propagated observational uncertainty and model ensemble spread. Negative values indicate net ocean CO_2 uptake. All fluxes are annual means expressed in Pg C yr^{-1}.

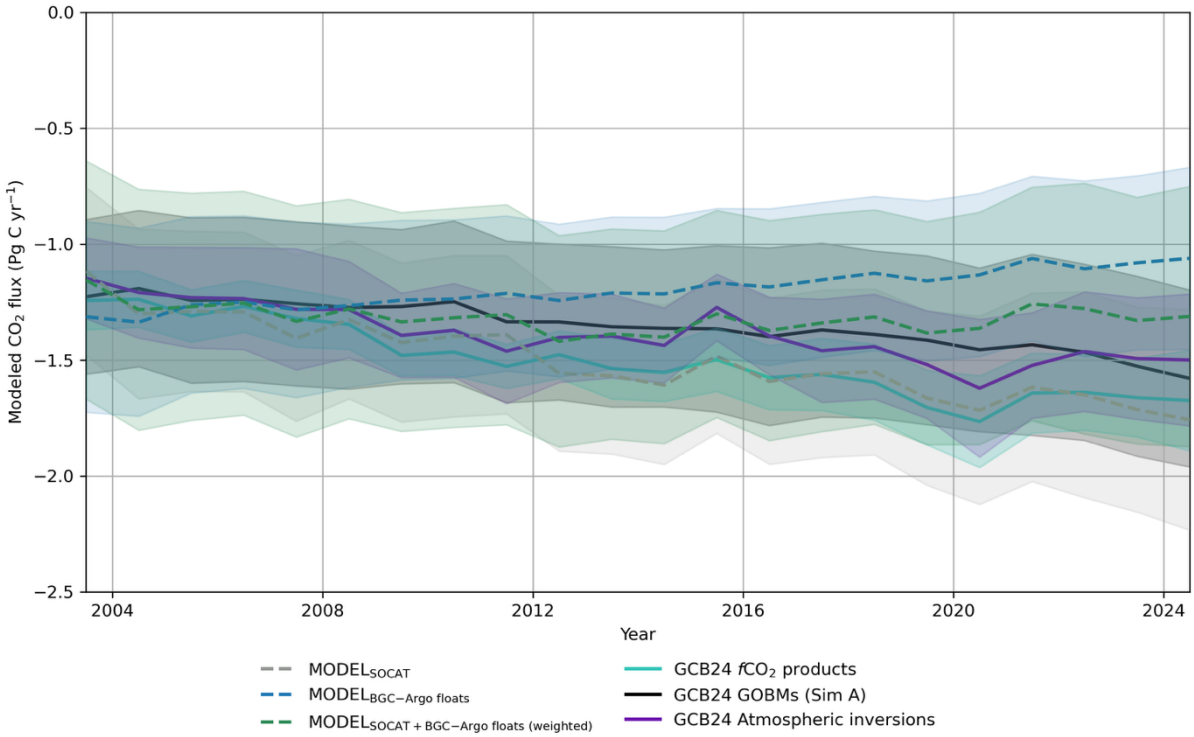


Figure 5. Southern Ocean CO_2 flux estimates south of 30°S for 2003–2024 from reconstruction-based and independent reference estimates including the SOCAT, BGC-Argo floats, and combined reconstructions (same colours as in Figure 4), Global Carbon Budget 2024 (GCB24; Friedlingstein et al., 2025) fCO_2-based products (turquoise), ocean biogeochemical models (GOBMs; black), and atmospheric inversion ensembles integrated south of 30°S (solid purple). Shaded regions indicate ±1σ uncertainty for each annual flux estimate: for the machine-learning reconstructions this reflects propagated observational and model uncertainty, while for GCB24 products it represents the inter-product standard deviation across the respective ensembles. Negative values indicate net ocean CO_2 uptake. All fluxes are annual means expressed in Pg C yr^{-1}.

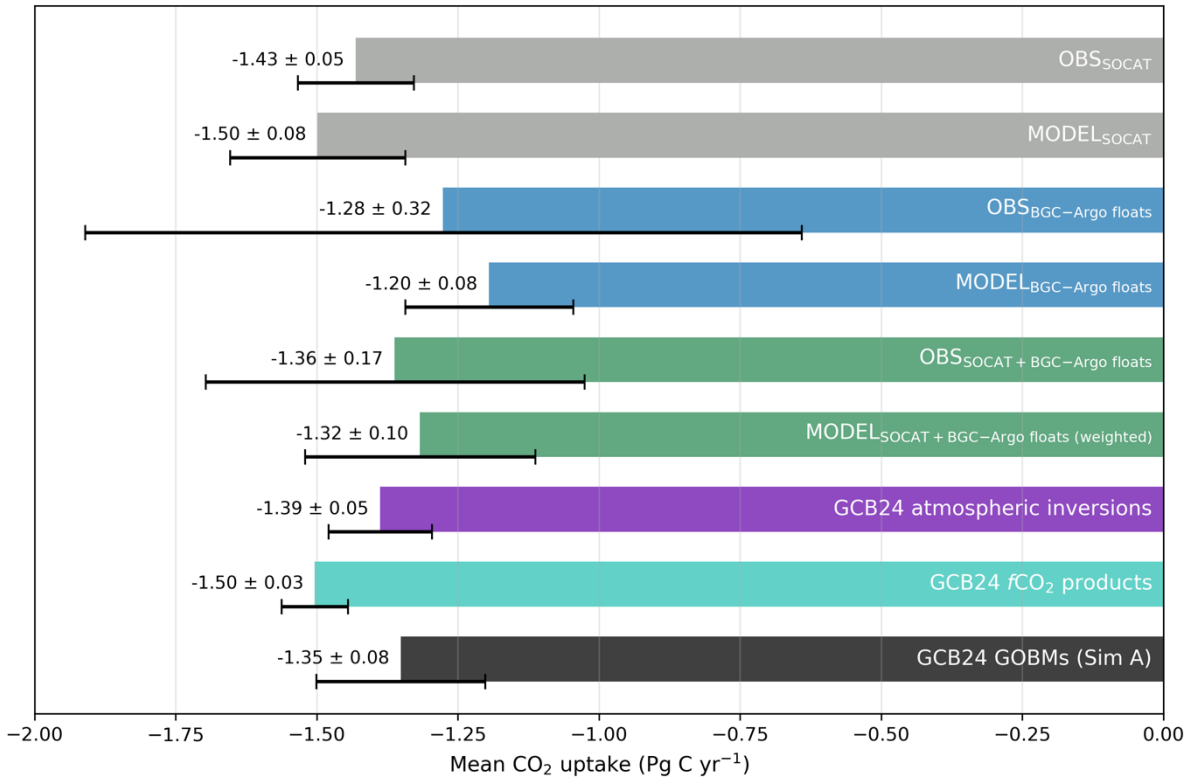


Figure 6. Mean annual Southern Ocean CO_2 uptake from multiple observational and modeling constraints for 2003–2024. Horizontal bars show the mean air–sea CO_2 flux south of 30°S over the period 2003–2024, expressed in Pg C yr^{-1}, with negative values denoting ocean uptake. Shown are observation-based flux estimates (OBS) derived directly from SOCAT, BGC-Argo floats, and their combined product, together with machine-learning reconstructions (Model) produced by MLP models trained on each observational dataset. Independent external constraints include Global Carbon Budget 2024 (Friedlingstein et al., 2025) ensemble estimates from atmospheric inversions, surface-ocean fCO_2 products, and Global Ocean Biogeochemical Models (GOBMs, Simulation A) evaluated south of 30°S. Error bars indicate 95 % confidence intervals of the mean derived from Monte Carlo propagation of annual flux uncertainties. Text labels report the mean ± propagated uncertainty of the mean.

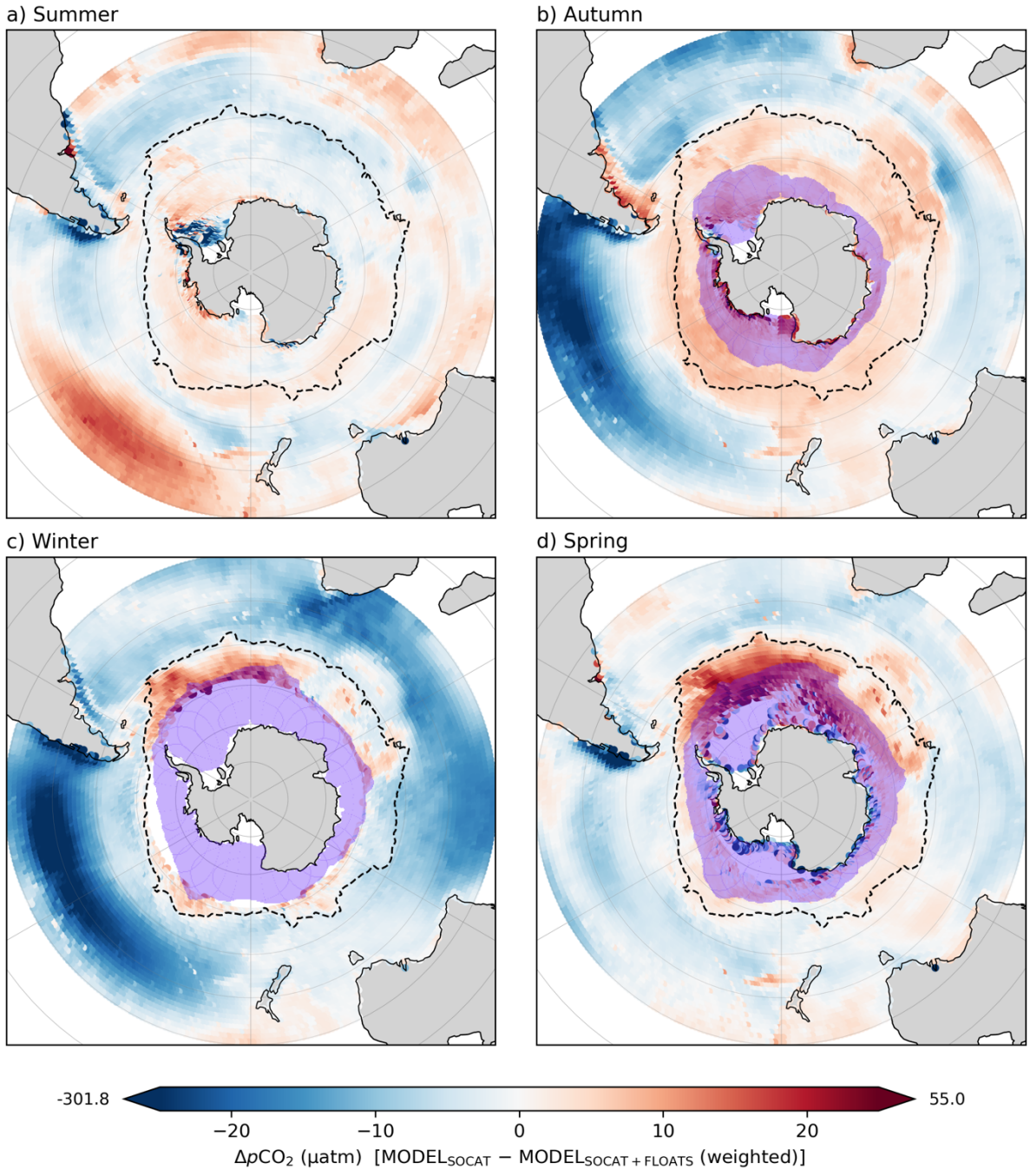


Figure 7. Seasonal mean differences in air–sea CO_2 flux (Pg C yr^{-1} equivalent; $MODEL_{SOCAT}$ − $MODEL_{SOCAT+BGC\text{-}Argo\ floats\ weighted}$) for the period 2003–2024, shown for austral summer (DJF), autumn (MAM), winter (JJA), and spring (SON). Positive values indicate regions where SOCAT-trained reconstructions estimate stronger CO_2 uptake than the uncertainty-weighted combined reconstruction. The climatological Polar Front is shown as the black dashed line (Park et al., 2019; Park and Durand, 2019). In autumn, winter and spring (panels (b), (c) and (d)), regions seasonally covered by sea ice are indicated by a purple shaded mask corresponding to grid cells where the maximum monthly sea-ice concentration exceeds 15%, delineating areas where open-ocean air–sea fluxes are not expected (sea ice climatology from OSI-SAF; Eastwood et al., 2011; Tonboe et al., 2011).

570

Dataset	**Slope (Pg C yr^{-2})**	***p*-value**
OBS_{SOCAT}	-0.037 ± 0.005	< 0.05
$OBS_{BGC\text{-}Argo\ floats}$	+0.030 ± 0.012	< 0.05
$OBS_{SOCAT+BGC\text{-}Argo\ floats}$	−0.013 ± 0.005	< 0.05
$MODEL_{SOCAT}$	−0.024 ± 0.002	< 0.05
$MODEL_{BGC\text{-}Argo\ floats}$	+0.012 ± 0.001	< 0.05
$MODEL_{SOCAT+BGC\text{-}Argo\ floats\ (weighted)}$	-0.003 ± 0.002	> 0.05
GCB24 fCO_2 products	−0.023 ± 0.002	< 0.05
GCB24 GOBMs SimA	−0.015 ± 0.001	< 0.05
GCB24 atmospheric inversions	−0.016 ± 0.002	< 0.05

571

572 **Table 2.** Linear trends (Pg C yr^{-2}) in annual mean Southern Ocean air–sea CO_2 fluxes derived from
573 observations (OBS_{SOCAT}, $OBS_{BGC\text{-}Argo\ floats}$, and $OBS_{SOCAT+BGC\text{-}Argo\ floats}$), corresponding machine-
574 learning reconstructions ($MODEL_{SOCAT}$, $MODEL_{BGC\text{-}Argo\ floats}$ and $MODEL_{SOCAT+BGC\text{-}Argo\ floats\ (weighted)}$), Global Carbon Budget (GCB) fCO_2-based products, GCB ocean biogeochemical models
576 (GOBMs, Simulation A), and atmospheric CO_2 inversions south of 30°S. Trends are estimated using
577 ordinary least squares regression and reported as slope ± standard error, with associated p-values.
578 Negative trends indicate a strengthening ocean CO_2 sink.

Dataset	**Sink growth (Pg C yr^{-1} decade^{-1}) over period (*p*-value)**		
	2003-2018 (Hauck et al., 2023a)	**2003 - 2012**	**2015 - 2024**
$MODEL_{SOCAT}$	−0.264 ± 0.035 (< 0.05)	−0.330 ± 0.068 (< 0.05)	−0.244 ± 0.052 (< 0.05)
$MODEL_{BGC\text{-}Argo\ floats}$	+0.111 ± 0.011 (< 0.05)	+0.101 ± 0.025 (< 0.05)	+0.129 ± 0.024 (< 0.05)
$MODEL_{SOCAT+BGC\text{-}Argo\ floats\ (weighted)}$	−0.087 ± 0.028 (< 0.05)	−0.179 ± 0.048 (< 0.05)	+0.042 ± 0.045 (> 0.05)

Table 3. Decadal Southern Ocean CO_2 sink growth rates (Pg C yr^{-1} decade^{-1}) derived from machine-learning reconstructions trained on SOCAT-only, BGC-Argo floats-only and their uncertainty-weighted combination, evaluated over three analysis windows (2003–2018; 2003–2012; 2015–2024). Values are reported as slope ± standard error (SE), with the associated two-sided *p*-value in parentheses.

3.1 Reconciling empirical constraints on Southern Ocean CO_2 uptake

We first consider fluxes computed directly from uninterpolated observations as a diagnostic of how sampling coverage shapes inferred basin-scale signals, before examining the mapped reconstructions as our primary flux estimates; as expected, the two approaches yield divergent perspectives on both the magnitude and trend of Southern Ocean CO_2 uptake over 2003–2024, although these differences largely overlap within their uncertainty envelopes (Fig. 4a; Tables 2–3). OBS_{SOCAT} surface measurements indicate a strong CO_2 sink of −1.43 ± 0.05 Pg C yr^{-1} (95% CI: -1.53 to -1.33 Pg C yr^{-1}; Fig. 6; Table S2 of the Supplementary Material, negative values indicate a flux from the atmosphere to the ocean) and a statistically significant intensification of −0.037 ± 0.005 Pg C yr^{-2} ($p < 0.05$; Table 2). In contrast, pCO_2 estimates derived from BGC-Argo floats yield a weaker mean CO_2 uptake of −1.28 ± 0.32 Pg C yr^{-1} (95% CI: -1.91 to -0.64 Pg C yr^{-1}; Fig. 6; Table S2 of the Supplementary Material) and a significant positive trend of +0.030 ± 0.012 Pg C yr^{-2} ($p < 0.05$; Table 2). While the confidence intervals of the mean uptake overlap, indicating broadly consistent estimates of the overall Southern Ocean sink magnitude (Fig. 6), the opposing trends inferred from ship- and float-based

observations are statistically distinct, highlighting fundamentally different perspectives on its recent evolution.

Placed within the broader literature, the SOCAT-based intensification aligns with ship-based mapping reconstructions that indicate a reinvigoration of the Southern Ocean CO_2 sink after the early 2000s (Landschützer et al., 2015; Gruber et al., 2019; Hauck et al., 2023a). Observation-based syntheses suggest that basin-integrated uptake strengthened by approximately 0.5–0.7 Pg C yr^{-1} between the early 2000s and early 2010s, following a wind-driven weakening during the 1980s–1990s (Le Quéré et al., 2007; Landschützer et al., 2015). More recent multi-product analyses likewise report a transition from stagnation in the 1990s to renewed uptake in the 2000s, albeit with a more modest net increase of ~0.2–0.3 Pg C yr^{-1} by the late 2010s (Mayot et al., 2023), although these estimates remain sensitive to evolving observational coverage in the Southern Ocean (Fay et al., 2025). Consistent with this reported range, the SOCAT-only reconstruction over 2003-2012 yields a negative flux trend of -0.330 ± 0.068 Pg C yr^{-1} $decade^{-1}$, indicating increased uptake (Table 3). When additional float constraints are incorporated, the trend moderates to -0.179 ± 0.048 Pg C yr^{-1} $decade^{-1}$, whereas the float-only reconstruction indicates a weak weakening of +0.101 ± 0.025 Pg C yr^{-1} $decade^{-1}$, highlighting the sensitivity of decadal trends to the underlying observational framework (Table 3).

For the 2003-2018 period, overlapping with Hauck et al. (2023a), the SOCAT-based reconstruction indicates a negative flux trend of -0.264 ± 0.035 Pg C yr^{-1} $decade^{-1}$ (Table 3), statistically indistinguishable from the -0.26 ± 0.06 Pg C yr^{-1} $decade^{-1}$ reported for pCO_2-product ensembles (Hauck et al., 2023a). By contrast, the float-only reconstruction shows a weakening of +0.111 ± 0.011 Pg C yr^{-1} $decade^{-1}$, opposite in sign to the SOCAT-based and multi-product estimates, whereas the uncertainty-weighted SOCAT and BGC-Argo floats reconstruction further attenuates the trend to -0.087 ± 0.028 Pg C yr^{-1} $decade^{-1}$ (Table 3). During the most recent decade (2015–2024), this divergence intensifies: the SOCAT-only reconstruction continues to indicate strengthening (-0.244 ± 0.052 Pg C yr^{-1} $decade^{-1}$; Table 3), whereas the float-only reconstruction shows a persistent weakening (+0.129 ± 0.024 Pg C yr^{-1} $decade^{-1}$;Table 3) and the uncertainty-weighted SOCAT and BGC-Argo floats reconstruction suggests a weak positive trend, but it is not statistically significant (+0.042 ± 0.045 Pg C yr^{-1} $decade^{-1}$; Table 3).

These phases of sink weakening and subsequent reinvigoration are now well documented across observations and reconstructions, and have been linked to variability in wind speed and sea-surface temperature extremes, which together explain 39 ± 4% of the carbon-sink anomaly trend during the 1990–2001 weakening phase and 41 ± 7% during the 2002–2019 strengthening phase (Landschützer et al., 2016; Gruber et al., 2023; Mignot et al., 2025). By contrast, the weakening trend inferred from float-derived pCO_2 estimates is consistent with recent analyses emphasizing wintertime and high-latitude processes, including enhanced outgassing south of the Polar Front associated with shifts in westerly wind position and surface buoyancy forcing (Keppler & Landschützer, 2019; Zhang et al., 2022). Enhanced wintertime outgassing south of the Polar Front is directly observed in regions with relatively strong winter ship coverage, such as the Drake Passage, and a climatological analysis for 1999–2019 confirms persistent winter

outgassing in this sector (Arbilla et al., 2024), supporting the interpretation that intensified high-latitude winter outgassing can partially offset summertime uptake and moderate basin-scale Southern Ocean CO_2 sink trends. Independent constraints further indicate that wintertime CO_2 outgassing in the Southern Ocean has been substantially underestimated in observation-based products lacking year-round coverage (Zhang et al., 2025), and that sparse, seasonally biased sampling can induce large positive biases in basin-scale uptake estimates and apparent trends (Hauck et al., 2023b).

Much of the apparent divergence in net flux trends and associated uncertainty envelopes can be reduced by applying the MLP-based reconstruction basin-scale averaging, leading to more consistent estimates of Southern Ocean CO_2 uptake across observational frameworks (Fig. 4b; Tables 2–3). All three machine-learning reconstructions yield comparable mean fluxes, ranging from -1.20 ± 0.08 Pg C yr^{-1} for the float-trained reconstruction (95% CI: −1.34 to −1.05 Pg C yr^{-1}; Fig. 6) to -1.50 ± 0.08 Pg C yr^{-1} for the SOCAT-trained reconstruction (95% CI: −1.65 to −1.34 Pg C yr^{-1}; Fig. 6), with the uncertainty-weighted combined reconstruction yielding -1.32 ± 0.10 Pg C yr^{-1} (95% CI: −1.53 to −1.12 Pg C yr^{-1}; Fig. 6). The reduced spread between observation-only and reconstruction-based estimates reflects not only improved spatiotemporal coverage but also the ability of the MLP-based reconstruction to account for differences in sampling seasonality and spatial coverage across observing systems before basin-scale integration. Float-derived pCO_2 estimates are associated with substantially larger pointwise uncertainty than ship-based measurements; however, this uncertainty is largely uncorrelated in space and time (Bittig et al., 2018; Heimdal & McKinley, 2024). The inclusion of unbiased but variable Argo-derived carbon observations can substantially reduce basin-scale uncertainty once integrated through mapping frameworks, as coherent physical signals are retained while random errors are averaged out (Heimdal & McKinley, 2024).

Here, we demonstrate this behavior in the real Southern Ocean, where float-derived pCO_2 is not synthetically prescribed but reflects actual sampling of wintertime and high-latitude (south of ~50–55°S) regimes. Seasonal time series of basin-mean pCO_2 from the three reconstructions (Fig. S15 of the Supplementary Material) further highlights the importance of this year-round sampling: float-based estimates exhibit systematically higher wintertime values and stronger seasonal contrasts than SOCAT-only reconstructions, while the combined reconstruction closely follows the float-derived seasonal evolution. This comparison illustrates how winter and high-latitude conditions, historically undersampled by ship-based observations, exert a strong influence on the basin-scale mean and its long-term evolution.

Across products, reconstruction-based estimates reduce uncertainty by ~78% for float-only constraints and by ~37% for combined SOCAT–float constraints, while SOCAT-only reconstructions exhibit an increase of ~41% in uncertainty relative to the dense ship-based observational product, likely because the reconstruction explicitly includes uncertainty associated with observational gaps, whereas observation-only basin means do not (Fig. 4). This demonstrates that large random errors in float-derived pCO_2 do not preclude their effective use in constraining basin-scale Southern Ocean CO_2 uptake.

3.2 Systematic uncertainty and observational limitations in float-derived CO_2 fluxes

The suppression of random observational noise through mapping does not, however, eliminate potential systematic errors in float-derived pCO_2. At present, float pCO_2 is not measured directly but inferred from temperature, salinity, and oxygen, and therefore inherits uncertainties associated with oxygen sensors, carbonate system parameterizations, and empirical mappings (Sauzède et al., 2017; Williams et al., 2017; Bittig et al., 2018; Carter et al., 2021). Direct intercomparisons between inferred and measured pCO_2 indicate systematic offsets of order 5–15 µatm under well-constrained conditions; for example, using a recovered profiling float equipped with a pCO_2 sensor near Cape Verde, Bittig et al. (2018) report mean biases of −9 ± 10 µatm for CANYON-B and +1 ± 12 µatm for CONTENT at 200 dbar, while poorly constrained deployments exhibit substantially larger deviations exceeding ±20–30 µatm, particularly near the surface (Bittig et al., 2018). Because such offsets are coherent in space and time, they cannot be removed through averaging and have been shown to induce substantial biases in reconstructed air–sea CO_2 fluxes if left unconstrained, leading to underestimation of the global ocean carbon sink by up to ~0.3 Pg C yr^{-1} (Heimdal & McKinley, 2024). Unlike float products that derive pCO_2 from pH measurements, which carry an additional systematic positive bias of ~15 ± 3 µatm driven by a negative offset in float pH (Zhang et al., 2026), the oxygen-based algorithms used here avoid this source of error, though the uncertainties described above remain.

To address these sources of uncertainty, the uncertainty-weighted combined reconstruction down-weights float-derived pCO_2 relative to SOCAT observations in proportion to their respective uncertainties, thereby limiting the influence of potential systematic float offsets while retaining the seasonal and latitudinal coverage provided by floats. In practice, this anchoring is achieved by training the reconstruction on a merged SOCAT–float dataset in which float-derived pCO_2 estimates are weighted by their propagated uncertainty relative to ship-based observations, ensuring that SOCAT measurements constrain the large-scale mean state while floats primarily inform undersampled seasons and regions. Notably, the difference between the mean fluxes from the float-trained and uncertainty-weighted combined reconstructions (≈0.12 Pg C yr^{-1}; Fig. 6; Table S2) is smaller than, but consistent with, the magnitude of systematic bias identified in observing system simulation experiments (~0.2–0.3 Pg C yr^{-1}; Heimdal & McKinley, 2024). This suggests that anchoring float-derived estimates to ship-based observations mitigates a substantial fraction of this bias while preserving physically informative wintertime signals. This combined framework is therefore designed to reduce both random uncertainty and systematic bias, yielding a more robust estimate of basin-scale Southern Ocean CO_2 uptake until direct pCO_2 measurements on autonomous platforms become available. Incorporating float-derived constraints also shifts the mean Southern Ocean CO_2 uptake from −1.50 to −1.32 Pg C yr^{-1} (a reduction of ~0.18 Pg C yr^{-1}, ≈12%; Fig. 6; Table S2). This shift exceeds the propagated uncertainty on each mean and is consistent with OSSE-based expectations (Hauck et al., 2023b) and satellite-based indications of underestimated winter outgassing in ship-dominated products (Zhang et al., 2025), though the uncertainty on the difference depends on covariance between reconstructions.

Together, these results indicate that the uncertainty-weighted combined reconstruction reconciles the opposing biases inherent to the individual observing systems, reducing the tendency of ship-only constraints to overestimate basin-scale uptake while correcting the weaker uptake inferred from float-only estimates. The resulting flux estimate falls within the range expected from independent observing system simulation experiments and process-based assessments, suggesting that combining complementary observation streams can recover a more balanced and physically consistent estimate of Southern Ocean CO_2 uptake.

Over the 2003-2024 period, trends inferred from the reconstructed fluxes are markedly weaker than those derived directly from the observation-only series (Fig. 4b; Table 2). The SOCAT-trained reconstruction exhibits a statistically significant strengthening of -0.024 ± 0.002 Pg C yr^{-2}, broadly consistent with expectations from increasing air–sea CO_2 disequilibrium under rising atmospheric CO_2 (Takahashi et al., 2009; Landschützer et al., 2015; Gruber et al., 2019). This signal likely reflects the longer temporal coverage of SOCAT, which extends back to the 1990s and was retained during model training even though flux trends are evaluated only over 2003–2024. The SOCAT-trained reconstruction therefore benefits from a longer training record for constraining low-frequency variability and secular increases in air–sea CO_2 disequilibrium, whereas float-based training is limited to the shorter post-2003 record, albeit with known seasonal and spatial sampling biases. The float-trained reconstruction retains a significant weakening trend ($+0.012 \pm 0.001$ Pg C yr^{-2}), which may reflect its stronger sensitivity to wintertime and high-latitude variability that is directly sampled by floats but only sparsely represented in ship-based observations (Table 2; Fig. S15 of the Supplementary Material). Seasonal maps from an additional summer-only trained reconstruction (Fig. S14 of the Supplementary Material) illustrate the limitations of training from floats without year-round coverage, showing unrealistic wintertime and ice-edge pCO_2 patterns when winter observations are not included. In contrast, seasonal basin-mean time series from the float-constrained reconstruction (Fig. S15) exhibit systematically higher winter values and stronger seasonal contrasts relative to SOCAT-only reconstructions, consistent with a stronger influence of wintertime regimes on its inferred long-term evolution. In contrast, the uncertainty-weighted combined reconstruction shows a small but not statistically significant trend over 2003–2024 (-0.003 ± 0.002 Pg C yr^{-2}), indicating that the opposing tendencies inferred from the individual observing systems largely cancel once seasonal and latitudinal sampling biases are mitigated and wintertime regimes are consistently represented. It should be noted, however, that BGC-Argo float density increased substantially over this period, such that the combined reconstruction transitions from being largely SOCAT-constrained in the early years to increasingly float-informed in later years, which may itself impart a residual trend-like influence on the reconstructed fluxes. With this caveat in mind, the results nonetheless suggest that, once seasonally complete sampling is accounted for, the basin-scale Southern Ocean CO_2 sink has remained approximately stable over the past two decades.

3.3 Physical drivers of sampling-dependency

The divergence between SOCAT- and float-derived Southern Ocean air–sea CO_2 flux estimates primarily reflects differences in the seasonal and latitudinal regimes sampled by each observing

system, rather than contradictory signals in basin-scale flux variability (Fig. 4a; Table 2). SOCAT observations are concentrated in austral summer and mid-latitude waters, where shallow mixed layers, strong stratification, and enhanced biological drawdown favor net CO_2 uptake (Fay et al., 2014; Bakker et al., 2016; Gray et al., 2018; Hauck et al., 2023b). In contrast, BGC-Argo floats routinely sample winter and high-latitude regimes in which air–sea CO_2 exchange is governed by deep mixing, ventilation of carbon-rich subsurface waters, and episodic outgassing. Float estimates reveal elevated wintertime surface pCO_2 south of the Polar Front, typically 5–20 µatm higher than summertime values, reflecting entrainment of dissolved inorganic carbon during deep winter mixing (Fig. S12 of the Supplementary Material; Gray et al., 2018; Bushinsky et al., 2019; Olivier & Haumann, 2025).

The uncertainty-weighted combined reconstruction provides a physically consistent basis for interpreting how these sampling differences translate into the basin-scale flux adjustment (Fig. 7). During austral summer, air–sea CO_2 exchange is relatively uniform across reconstructions, yielding broadly similar uptake and only modest, spatially diffuse differences. Comparison of the summer panel in Fig. 7 shows that differences between SOCAT-only and combined reconstructions are already present during summer but remain smaller than the pronounced winter adjustments, indicating that the basin-scale correction does not arise solely from the inclusion of winter observations and also reflects more subtle differences in the representation of summer fluxes.

In contrast, during autumn and winter the combined reconstruction reveals spatially coherent reductions in inferred uptake across high-latitude regions. These seasonal adjustments dominate the annual-mean flux correction, indicating that the revised Southern Ocean CO_2 uptake reflects the integrated influence of high-latitude ventilation regimes captured by float observations rather than a uniform offset applied across seasons or regions. Some regional anomalies may additionally reflect residual sampling heterogeneity, particularly in sparsely sampled sectors evident in the seasonal coverage of SOCAT and BGC-Argo observations (Fig. 1); however, the persistence of the wintertime signal across independently sampled regions and seasons indicates that the dominant adjustment arises from coherent high-latitude ventilation processes rather than data sparsity alone.

Wind-driven variability further amplifies the seasonal difference between summer and winter air-sea CO_2 exchange. Across autumn and especially winter (Fig. 7b-c), positive anomalies dominate south of the Polar Front, indicating regions where the SOCAT-trained reconstruction estimates stronger CO_2 uptake than the uncertainty-weighted combined reconstruction. This pattern shows that inclusion of float observations systematically reduces inferred uptake by resolving winter periods of intensified westerlies, more frequent during austral winter, enhance Ekman divergence, storm-driven vertical mixing, and the upwelling of carbon-rich deep waters, promoting transient outgassing over broad high-latitude sectors (Lenton et al., 2009; Nicholson et al., 2022; Menviel et al., 2023). The alignment of high-wind ventilation regions with reduced uptake in the combined reconstruction (Fig. 7c) indicates that float-resolved wintertime outgassing drives the basin-scale adjustment. Beyond their role in resolving surface pCO_2 variability, autonomous platforms also offer a promising pathway toward improved *in*

situ characterization of air–sea forcing, as emerging float and surface-vehicle technologies enable concurrent estimates of near-surface winds and momentum fluxes, strengthening their potential as complementary constraints to ship-based SOCAT observations in future observing systems (Delaigue et al., 2026a).

Seasonal biological compensation provides an additional explanation for the differences between reconstructions. Differences between reconstructions are comparatively small during summer (Fig. 7a), when stratified conditions and biological drawdown dominate and both observing systems sample similar regimes. By contrast, the strongest adjustments occur outside the peak growing season, particularly during winter and spring (Fig. 7c–d), indicating that the annual-mean reduction in uptake arises from processes operating during the ventilated season rather than from changes in summer productivity. While SOCAT primarily resolves periods of maximum biological drawdown during summer, floats capture the subsequent autumn and winter remineralization of organic matter and respiration-driven CO_2 release (Arrigo et al., 2008; Siegel et al., 2014). The seasonal structure of Figure 7 therefore indicates that strong summer uptake is partially offset by enhanced winter outgassing when year-round sampling is included, yielding a weaker annual-mean sink in the combined reconstruction. Regional process studies further document an intensified summer sink in Antarctic coastal waters after 2012, linked to enhanced biological drawdown and stratification-driven suppression of vertical carbon supply (Monteiro et al., 2020). This enhanced summer uptake likely reflects, in part, preceding winter strengthening of westerly winds that increases nutrient supply through upwelling and fuels subsequent spring–summer productivity. When sampled in isolation, these summer conditions emphasize strong uptake, whereas inclusion of the full seasonal cycle reveals substantial compensation that suppresses the annual mean sink. Consistent with this interpretation, year-round observations in the Drake Passage indicate near-equilibrium annual air–sea CO_2 exchange (1.3 ± 15.5 Tg C yr^{-1} over 1999–2019), with regions south of the Southern Antarctic Circumpolar Current Front acting as a persistent annual CO_2 source driven primarily by non-thermal controls on surface pCO_2 and wintertime ventilation of carbon-rich waters (Arbilla et al., 2024).

High-latitude regimes inaccessible to routine ship operations further accentuate these differences observed between the SOCAT-only and combined reconstructions. The largest positive differences (SOCAT reconstruction fluxes > combined reconstruction fluxes; Fig. 7) occur south of the Polar Front and within the Antarctic Zone (Fig. 7b–c), including regions adjacent to the marginal ice zone masked in winter (Fig. 7c). Floats routinely sample the marginal ice zone, the Antarctic Zone, and dynamically active Polar Front regions characterized by strong lateral and vertical gradients in pCO_2 and gas exchange (Fig. 1). These environments are sparsely represented in SOCAT (Fig. 1) but exhibit some of the largest seasonal amplitudes in air–sea CO_2 flux (Fig. 7; Bakker et al., 2016; Bushinsky et al., 2019; Roobaert et al., 2019). Their inclusion by floats introduces enhanced variance and systematic wintertime flux anomalies into basin-integrated estimates. Thus, by jointly representing summer biological drawdown and winter ventilation regimes, the combined SOCAT + BGC-Argo floats framework may provide the physical basis for reconciling the divergent

observational perspectives and for recovering a more representative basin-scale Southern Ocean CO_2 flux (Fig. 4b).

3.4 Constraining the magnitude of the Southern Ocean carbon sink

The Global Carbon Budget (GCB) provides three complementary classes of estimates for Southern Ocean air–sea CO_2 exchange, each grounded in distinct methodological constraints (Fig. 5). Over 2003–2024, these approaches imply broadly similar but non-identical mean sinks south of 30°S, ranging from -1.35 ± 0.08 Pg C yr^{-1} in global ocean biogeochemical models (GOBMs) to -1.39 ± 0.05 Pg C yr^{-1} in atmospheric inversion ensembles, with fCO_2-based products indicating somewhat stronger uptake of -1.50 ± 0.03 Pg C yr^{-1} (Fig. 6).

As emphasized in the GCB, these differences in estimates of Southern Ocean air-sea CO_2 flux arise from the distinct constraints applied by each approach. Atmospheric inversions infer regional fluxes by closing the global atmospheric CO_2 budget and are therefore tightly constrained at the global scale but rely on atmospheric transport and prior flux distributions to partition uptake regionally. GOBMs simulate Southern Ocean CO_2 uptake prognostically from physical circulation and biogeochemical processes, yielding fluxes that are internally consistent with large-scale ocean dynamics but not explicitly optimized to match regional surface fCO_2 observations. In addition, GOBM estimates need to correct from pre-industrial sources of CO_2 to the atmosphere from river input to the ocean, which is a major source of uncertainty of regional estimates, and in particular of the Southern Ocean net flux estimate (Friedlingstein et al., 2025). Finally, fCO_2-based products reconstruct air–sea CO_2 exchange by statistically mapping surface ocean fCO_2 observations. As a result, they rely heavily on the SOCAT database, inheriting its seasonal and spatial sampling structure and emphasizing summer and mid-latitude regimes characterized by strong biological drawdown.

Within this framework, the reconstructed fluxes are within the range of independent constraints provided by the different classes of Global Carbon Budget estimates (Fig. 5; Friedlingstein et al., 2025). The SOCAT-trained reconstruction yields a mean Southern Ocean CO_2 uptake of -1.50 ± 0.08 Pg C yr^{-1}, closely matching the GCB fCO_2-based products, as expected given their shared reliance on ship-based surface observations and similar seasonal sampling structure. By contrast, the float-trained reconstruction yields a substantially weaker mean sink of -1.20 ± 0.08 Pg C yr^{-1}, lying toward the weak-uptake edge of the range spanned by GCB estimates (Fig. 6). This divergence reflects the enhanced sensitivity of float-derived pCO_2 to high-latitude and winter processes that are weakly constrained in SOCAT-based products but indirectly integrated in atmospheric inversions and GOBMs through global mass balance and circulation constraints.

Taken together, these end-member reconstructions highlight the limits of relying on any single observing system to infer basin-scale Southern Ocean CO_2 uptake. The uncertainty-weighted combined reconstruction reconciles these opposing tendencies by jointly representing summer biological drawdown and winter ventilation within a seasonally and latitudinally (almost) complete framework. Its resulting mean uptake of -1.32 ± 0.10 Pg C yr^{-1} lies between the

SOCAT- and float-trained extremes and within the range implied by atmospheric inversions and GOBMs. In terms of long-term change, SOCAT-based observations and reconstructions show the closest agreement with Global Carbon Budget estimates, all of which indicate a statistically significant intensification of the Southern Ocean CO_2 sink since the early 2000s (-0.037 ± 0.005 Pg C yr^{-2} for SOCAT observations; -0.024 ± 0.002 Pg C yr^{-2} for the SOCAT-trained reconstruction; -0.023 to -0.015 Pg C yr^{-2} across GCB fCO_2 products, GOBMs, and atmospheric inversions; Table 2). However, because these large-scale constraints are governed primarily by global mass balance and large-scale circulation, they may not fully capture regional seasonal and high-latitude processes that strongly influence Southern Ocean air–sea CO_2 exchange and its recent variability.

Notably, the near-zero trend inferred from the uncertainty-weighted combined reconstruction remains broadly consistent with independent evidence that Southern Ocean outgassing variability has partially offset expected sink intensification over recent decades, particularly in upwelling-favourable high-latitude regions (Olivier & Haumann, 2025). Atmospheric inversions and GOBMs integrate these compensating regional signals into a net intensifying sink driven by rising atmospheric CO_2 and large-scale circulation, whereas the observation-based reconstructions presented here emphasize how regional ventilation and seasonal processes can modulate or temporarily offset this expected increase. Reconciling these perspectives likely requires a more explicit regional attribution of trends across upwelling- and downwelling-dominated sectors of the Southern Ocean, an analysis beyond the scope of the present study but essential for interpreting long-term changes in basin-scale carbon uptake.

Nonetheless, in terms of absolute magnitude, our results indicate that, once seasonal and latitudinal sampling biases are removed, the Southern Ocean CO_2 mean sink south of 30°S is -1.32 ± 0.10 Pg C yr^{-1} over 2003–2024, as inferred from the uncertainty-weighted combined reconstruction using SOCAT and BGC-Argo floats. This estimate lies toward the weaker end of, but remains consistent with, the range implied by atmospheric inversions and global ocean biogeochemical models (≈ -1.3 to -1.4 Pg C yr^{-1}), which are constrained by global mass balance and large-scale circulation, and therefore emphasize physical controls that are also directly sampled by floats. Relative to GCB fCO_2-based products (-1.50 ± 0.03 Pg C yr^{-1}), correcting for the strong seasonal and latitudinal sampling biases inherent to ship-based observations reduces the inferred basin-scale sink by ~0.18 Pg C yr^{-1} (≈12%), comparable to the reduction obtained when correcting SOCAT-only reconstructions and consistent with independent observing system simulation experiments and algorithm-based studies that quantify the impact of sparse and seasonally biased sampling on Southern Ocean CO_2 uptake estimates (Hauck et al., 2023b; Zhang et al., 2025).

In contrast to the individual SOCAT- and float-based reconstructions, which exhibit statistically significant intensifying and weakening trends, respectively, the uncertainty-weighted combined reconstruction shows a small, not statistically significant long-term trend over 2003–2024 (-0.003 ± 0.002 Pg C yr^{-2}; $p > 0.05$; Table 2). Thus, the opposing tendencies inferred from ship- and float-based observations appear to largely cancel once seasonal and latitudinal sampling biases are accounted for. This suggests that, when year-round and high-

latitude regimes are consistently represented, the basin-scale Southern Ocean CO_2 sink has remained approximately stable over the past two decades.

4. Conclusions

The Southern Ocean remains one of the most consequential yet most uncertain components of the global carbon cycle, in large part because its air–sea CO_2 exchange is inferred from an observing system that is sparse, uneven, and continually evolving. Here we combine SOCAT observations with surface pCO_2 estimates from BGC-Argo floats to quantify how expanded autonomous sampling alters basin-scale Southern Ocean CO_2 flux estimates south of 30°S over 2003–2024.

Across observation-only time series, ship- and float-derived constraints suggest markedly different pictures of the Southern Ocean sink: SOCAT implies a strong mean CO_2 uptake and a pronounced strengthening of this uptake over time, whereas floats imply a weaker sink and, in isolation, an apparent weakening trend. These differences primarily reflect systematic sampling of different seasonal and latitudinal regimes rather than incompatible basin-scale behaviour. When combined within an MLP reconstruction framework that reduces sampling biases, the inferred Southern Ocean CO_2 sink weakens relative to SOCAT-dominated products and the apparent long-term trend largely vanishes, yielding a near-stable basin-scale sink consistent with evidence that enhanced high-latitude outgassing and ventilation can partially offset expected sink intensification over recent decades. While Global Carbon Budget fCO_2 products, GOBMs, and atmospheric inversions generally indicate a strengthening Southern Ocean sink, the combined reconstruction suggests that regionally heterogeneous change, particularly across upwelling- and downwelling-dominated sectors, may damp the net basin-scale trend, highlighting the need for explicit regional attribution of long-term change.

The uncertainty-weighted combined reconstruction, representing the most physically complete observational constraint presented here, yields a mean Southern Ocean CO_2 uptake of -1.32 ± 0.10 Pg C yr^{-1} over 2003–2024 with only a small long-term trend. Relative to SOCAT-dominated products and SOCAT-only reconstructions, explicitly correcting for sampling bias reduces the inferred basin-scale sink by ~0.18 Pg C yr^{-1} (≈12%), consistent with observing system simulation experiments and independent evidence for underestimated wintertime outgassing. The resulting estimate remains observation-based yet is physically interpretable and broadly consistent with atmospheric inversion and global ocean biogeochemical model constraints synthesized in the Global Carbon Budget. Overall, these results indicate that a substantial fraction of previously reported multi-decadal strengthening in SOCAT-dominated products can arise from observing-system sampling structure rather than basin-scale change, and that integrating complementary observation streams provides a practical pathway toward more robust carbon-cycle monitoring in the Southern Ocean.

Nevertheless, key uncertainties remain. A first priority is continued reduction of uncertainty in float-derived pCO_2 through direct pCO_2 measurements on autonomous platforms and sustained co-validation with ship-based reference observations. Such efforts will tighten uncertainty, better constrain potential systematic offsets, and progressively reduce reliance on algorithmic

carbonate-system reconstructions. This also requires exploiting the complementary strengths of emerging autonomous observing platforms, including uncrewed surface vehicles such as saildrones, which can provide direct surface pCO_2 and air–sea forcing measurements for cross-validation of float-derived estimates, while profiling floats uniquely resolve the vertical structure connecting surface fluxes to subsurface carbon reservoirs. Together, these platforms offer a pathway toward an observing system that is both vertically resolved and directly traceable to surface reference measurements, even under harsh winter conditions that remain difficult to sample by ships alone.

A second priority is defining the optimal balance between autonomous and ship-based sampling as the observing system evolves. Future observing-system simulation experiments explicitly designed around mixed ship–float strategies, together with sustained cross-calibration efforts, will be critical for maintaining an observing system that is both spatially complete and metrologically anchored. Only through such an integrated, cross-validated observing system will it become possible to distinguish true climate-driven changes in Southern Ocean CO_2 uptake from artifacts of an evolving observing network, enabling the Southern Ocean to serve as a robust benchmark for tracking the trajectory of the global ocean carbon sink in a changing climate.

Funding

The research leading to these results has received part of the funding from the European Union's Horizon research and innovation program under grant N°101188028 (TRICUSO project). REFINE has received funding from the European Research Council (ERC) under the European Union's Horizon 2020 research and innovation programme (grant agreement N° 834177). Argo-2030 has received the support of the French government within the framework of the "Investissements d'avenir" program integrated in France 2030 and managed by the Agence Nationale de la Recherche (ANR) under the reference "ANR-21-ESRE-0019".

Data Availability Statement

All data and code used in this analysis are available in Delaigue (2026b). Figures were made with Python version 3.9 (van Rossum & Drake Jr, 2009).

Author Contributions

HC, LD, and RS conceptualized the project. LD curated the data. LD and RS conceptualized the methodology. LD used the necessary software, visualized the data, and prepared the original draft of the paper. HC, LD, PL, and RS performed the investigation. CWR, HC, JBS, LA, LD, PL, RS and SB reviewed and edited the paper.

Acknowledgements

We thank the many scientists, technicians, and data managers involved in the global Surface Ocean CO_2 Atlas (SOCAT) and the Biogeochemical Argo (BGC-Argo) programs for their sustained efforts in data collection, curation, and quality control. These community-driven initiatives provide the essential observational foundation for this work, and we are especially grateful that the datasets are made freely

available through the SOCAT portal and the Copernicus Marine Service. The OneArgo data were collected and made freely available by the International Argo Program and the national programs that contribute to it (https://argo.ucsd.edu, https://www.ocean-ops.org). The OneArgo Program is part of the Global Ocean Observing System. We acknowledge the Ocean and Sea Ice Satellite Application Facility (OSI SAF) High Latitude Processing Center for producing and making available their reprocessing data sets and derived products from the Danish Meteorological Institute (DMI) and the Norwegian Meteorological Institute (MET Norway).

Conflict of Interest

The contact author has declared that neither they nor their co-authors have any competing interests.

References

Arbilla, L. A., Ruiz-Etcheverry, L. A., López-Abbate, C., & Kahl, L. C. (2024). CO2 sink and source zones delimited by marine fronts in the Drake Passage. *Progress in Oceanography*, *223*, 103246. https://doi.org/https://doi.org/10.1016/j.pocean.2024.103246

Arrigo, K. R., van Dijken, G. L., & Bushinsky, S. (2008). Primary production in the Southern Ocean, 1997–2006. *Journal of Geophysical Research: Oceans*, *113*(C8). https://doi.org/https://doi.org/10.1029/2007JC004551

Bakker, D. C. E., Pfeil, B., O'Brien, K. M., Currie, K. I., Jones, S. D., Landa, C. S., Lauvset, S. K., Metzl, N., Munro, D. R., Nakaoka, S.-I., Olsen, A., Pierrot, D., Saito, S., Smith, K., Sweeney, C., Takahashi, T., Wada, C., Wanninkhof, R., Alin, S. R.,…Woosley, R. (2016). Surface Ocean CO2 Atlas (SOCAT) V4. In: PANGAEA.

Behncke, J., Ilyina, T., Chegini, F., & Landschützer, P. (2026). Improved air-sea CO₂ flux estimates from sailboat measurements. *Science Advances*, *12*(2), eadz1502. https://doi.org/doi:10.1126/sciadv.adz1502

Behncke, J., Landschützer, P., & Tanhua, T. (2024). A detectable change in the air-sea CO2 flux estimate from sailboat measurements. *Scientific reports*, *14*(1), 3345. https://doi.org/10.1038/s41598-024-53159-0

Bittig, H. C., Maurer, T. L., Plant, J. N., Schmechtig, C., Wong, A. P. S., Claustre, H., Trull, T. W., Udaya Bhaskar, T. V. S., Boss, E., Dall'Olmo, G., Organelli, E., Poteau, A., Johnson, K. S., Hanstein, C., Leymarie, E., Le Reste, S., Riser, S. C., Rupan, A. R., Taillandier, V.,…Xing, X. (2019). A BGC-Argo Guide: Planning, Deployment, Data Handling and Usage [Review]. *Frontiers in Marine Science*, *6*. https://doi.org/10.3389/fmars.2019.00502

Bittig, H. C., Steinhoff, T., Claustre, H., Fiedler, B., Williams, N. L., Sauzède, R., Körtzinger, A., & Gattuso, J.-P. (2018). An alternative to static climatologies: Robust estimation of open ocean CO2 variables and nutrient concentrations from T, S, and O2 data using Bayesian neural networks. *Frontiers in Marine Science*, *5*, 328. https://doi.org/https://doi.org/10.3389/fmars.2018.00328

Bushinsky, S. M., Landschützer, P., Rödenbeck, C., Gray, A. R., Baker, D., Mazloff, M. R., Resplandy, L., Johnson, K. S., & Sarmiento, J. L. (2019). Reassessing Southern Ocean Air-Sea CO2 Flux Estimates With the Addition of Biogeochemical Float Observations. *Global Biogeochemical Cycles*, *33*(11), 1370-1388. https://doi.org/https://doi.org/10.1029/2019GB006176

Bushinsky, S. M., Nachod, Z., Fassbender, A. J., Tamsitt, V., Takeshita, Y., & Williams, N. (2025). Offset Between Profiling Float and Shipboard Oxygen Observations at Depth Imparts Bias on Float pH and Derived pCO2. *Global Biogeochemical Cycles*, *39*(5), e2024GB008185. https://doi.org/https://doi.org/10.1029/2024GB008185

Carter, B. R., Bittig, H. C., Fassbender, A. J., Sharp, J. D., Takeshita, Y., Xu, Y.-Y., Álvarez, M., Wanninkhof, R., Feely, R. A., & Barbero, L. (2021). New and updated global empirical seawater property estimation routines. *Limnology and Oceanography: Methods*, *19*(12), 785-809. https://doi.org/https://doi.org/10.1002/lom3.10461

Chai, F., Johnson, K. S., Claustre, H., Xing, X., Wang, Y., Boss, E., Riser, S., Fennel, K., Schofield, O., & Sutton, A. (2020). Monitoring ocean biogeochemistry with autonomous platforms. *Nature Reviews Earth & Environment*, *1*(6), 315-326. https://doi.org/10.1038/s43017-020-0053-y

Chikamoto, M. O., & DiNezio, P. (2021). Multi-Century Changes in the Ocean Carbon Cycle Controlled by the Tropical Oceans and the Southern Ocean. *Global Biogeochemical Cycles*, *35*(12), e2021GB007090. https://doi.org/https://doi.org/10.1029/2021GB007090

Claustre, H., Johnson, K. S., & Takeshita, Y. (2020). Observing the global ocean with biogeochemical-Argo. *Annual Review of Marine Science*, 23-48.

Delaigue, L., Cauchy, P., Cazau, D., Bonnel, J., Pensieri, S., Bozzano, R., Gros-Martial, A., Schaeffer, C., David, A., Stil, P., Poteau, A., Schmechtig, C., Leymarie, E., & Claustre, H. (2026a). Passive acoustic monitoring from profiling floats as a pathway to scalable autonomous observations of global surface wind. *Ocean Sci.*, *22*(1), 101-117. https://doi.org/10.5194/os-22-101-2026

Delaigue, L. (2026b). louisedelaigue/SOCAT-FLOATS-SO-SINK: Release for submission to journal (v0.0). Zenodo. https://doi.org/10.5281/zenodo.18935339

Denvil-Sommer, A., Gehlen, M., & Vrac, M. (2021). Observation system simulation experiments in the Atlantic Ocean for enhanced surface ocean pCO2 reconstructions. *Ocean Sci.*, *17*(4), 1011-1030. https://doi.org/10.5194/os-17-1011-2021

DeVries, T., & Deutsch, C. (2014). Large-scale variations in the stoichiometry of marine organic matter respiration. *Nature Geoscience*, *7*(12), 890-894. https://doi.org/10.1038/ngeo2300

Dong, Y., Bakker, D. C. E., Bell, T. G., Yang, M., Landschützer, P., Hauck, J., Rödenbeck, C., Kitidis, V., Bushinsky, S. M., & Liss, P. S. (2024). Direct observational evidence of strong CO₂ uptake in the Southern Ocean. *Science Advances*, *10*(30), eadn5781. https://doi.org/doi:10.1126/sciadv.adn5781

Eastwood, S., Larsen, K. R., Lavergne, T., Nielsen, E., Tonboe, R. Global Sea Ice Concentration Reprocessing. Product User Manual, Product OSI-409, Document version: 1.3, Data set version: 1.1, October 2011.

Fay, A. R., Gregor, L., Landschützer, P., McKinley, G. A., Gruber, N., Gehlen, M., Iida, Y., Laruelle, G. G., Rödenbeck, C., Roobaert, A., & Zeng, J. (2021). SeaFlux: harmonization of air–sea CO2 fluxes from surface pCO2 data products using a standardized approach. *Earth Syst. Sci. Data*, *13*(10), 4693-4710. https://doi.org/10.5194/essd-13-4693-2021

Fay, A. R., Heimdal, T. H., Acquaviva, V., Shaum, A. P., & McKinley, G. A. (2025). Sensitivity of Ocean Carbon Sink Estimates to Rare Observations. *Geophysical Research Letters*, *52*(19), e2025GL117961. https://doi.org/https://doi.org/10.1029/2025GL117961

Fay, A. R., McKinley, G. A., & Lovenduski, N. S. (2014). Southern Ocean carbon trends: Sensitivity to methods. *Geophysical Research Letters*, *41*(19), 6833-6840. https://doi.org/https://doi.org/10.1002/2014GL061324

Flanders Marine Institute (2021). Global Oceans and Seas, version 1. Available online at https://www.marineregions.org/. https://doi.org/10.14284/542

Friedlingstein, P., O'Sullivan, M., Jones, M. W., Andrew, R. M., Hauck, J., Landschützer, P., Le Quéré, C., Li, H., Luijkx, I. T., Olsen, A., Peters, G. P., Peters, W., Pongratz, J., Schwingshackl, C., Sitch, S., Canadell, J. G., Ciais, P., Jackson, R. B., Alin, S. R.,…Zeng, J. (2025). Global Carbon Budget 2024. *Earth Syst. Sci. Data*, *17*(3), 965-1039. https://doi.org/10.5194/essd-17-965-2025

Gloege, L., McKinley, G. A., Landschützer, P., Fay, A. R., Frölicher, T. L., Fyfe, J. C., Ilyina, T., Jones, S., Lovenduski, N. S., Rodgers, K. B., Schlunegger, S., & Takano, Y. (2021). Quantifying Errors in Observationally Based Estimates of Ocean Carbon Sink Variability. *Global Biogeochemical Cycles*, *35*(4), e2020GB006788. https://doi.org/https://doi.org/10.1029/2020GB006788

Gray, A. R., Johnson, K. S., Bushinsky, S. M., Riser, S. C., Russell, J. L., Talley, L. D., Wanninkhof, R., Williams, N. L., & Sarmiento, J. L. (2018). Autonomous biogeochemical floats detect significant carbon dioxide outgassing in the high-latitude Southern Ocean. *Geophysical Research Letters*, *45*(17), 9049-9057.

Gruber, N., Bakker, D. C. E., DeVries, T., Gregor, L., Hauck, J., Landschützer, P., McKinley, G. A., & Müller, J. D. (2023). Trends and variability in the ocean carbon sink. *Nature Reviews Earth & Environment*, *4*(2), 119-134. https://doi.org/10.1038/s43017-022-00381-x

Gruber, N., Landschützer, P., & Lovenduski, N. S. (2019). The Variable Southern Ocean Carbon Sink. *Annual Review of Marine Science*, *11*(1), 159-186. https://doi.org/10.1146/annurev-marine-121916-063407

Hauck, J., Gregor, L., Nissen, C., Patara, L., Hague, M., Mongwe, P., Bushinsky, S., Doney, S. C., Gruber, N., Le Quéré, C., Manizza, M., Mazloff, M., Monteiro, P. M. S., & Terhaar, J. (2023a). The Southern Ocean Carbon Cycle 1985–2018: Mean, Seasonal Cycle, Trends, and Storage. *Global Biogeochemical Cycles*, *37*(11), e2023GB007848. https://doi.org/https://doi.org/10.1029/2023GB007848

Hauck, J., Nissen, C., Landschützer, P., Rödenbeck, C., Bushinsky, S., & Olsen, A. (2023b). Sparse observations induce large biases in estimates of the global ocean CO₂ sink: an ocean model subsampling experiment. *Philosophical Transactions of the Royal Society A: Mathematical, Physical and Engineering Sciences*, *381*(2249), 20220063. https://doi.org/doi:10.1098/rsta.2022.0063

Hauck, J., Völker, C., Wolf-Gladrow, D. A., Laufkötter, C., Vogt, M., Aumont, O., Bopp, L., Buitenhuis, E. T., Doney, S. C., Dunne, J., Gruber, N., Hashioka, T., John, J., Quéré, C. L., Lima, I. D., Nakano, H., Séférian, R., & Totterdell, I. (2015). On the Southern Ocean CO2 uptake and the role of the biological carbon pump in the 21st century. *Global Biogeochemical Cycles*, *29*(9), 1451-1470. https://doi.org/https://doi.org/10.1002/2015GB005140

Heimdal, T. H., & McKinley, G. A. (2024). The importance of adding unbiased Argo observations to the ocean carbon observing system. *Scientific reports*, *14*(1), 19763. https://doi.org/10.1038/s41598-024-70617-x

Heimdal, T. H., McKinley, G. A., Sutton, A. J., Fay, A. R., & Gloege, L. (2024). Assessing improvements in global ocean pCO2 machine learning reconstructions with Southern Ocean autonomous sampling. *Biogeosciences*, *21*(8), 2159-2176. https://doi.org/10.5194/bg-21-2159-2024

Ho, D. T., Law, C. S., Smith, M. J., Schlosser, P., Harvey, M., & Hill, P. (2006). Measurements of air-sea gas exchange at high wind speeds in the Southern Ocean: Implications for global parameterizations. *Geophysical Research Letters*, *33*(16).

IPCC. (2023). *Climate Change 2021 – The Physical Science Basis: Working Group I Contribution to the Sixth Assessment Report of the Intergovernmental Panel on Climate Change*. Cambridge University Press. https://doi.org/DOI: 10.1017/9781009157896

Johnson, K., & Claustre, H. (2016). Bringing biogeochemistry into the Argo age. *Eos, Transactions American Geophysical Union*.

Keppler, L., & Landschützer, P. (2019). Regional Wind Variability Modulates the Southern Ocean Carbon Sink. *Scientific reports*, *9*(1), 7384. https://doi.org/10.1038/s41598-019-43826-y

Khatiwala, S., Tanhua, T., Mikaloff Fletcher, S., Gerber, M., Doney, S. C., Graven, H. D., Gruber, N., McKinley, G. A., Murata, A., Ríos, A. F., & Sabine, C. L. (2013). Global ocean storage of anthropogenic carbon. *Biogeosciences*, *10*(4), 2169-2191. https://doi.org/10.5194/bg-10-2169-2013

Landschützer, P., Gruber, N., & Bakker, D. C. E. (2016). Decadal variations and trends of the global ocean carbon sink. *Global Biogeochemical Cycles*, *30*(10), 1396-1417. https://doi.org/https://doi.org/10.1002/2015GB005359

Landschützer, P., Gruber, N., Haumann, F. A., Rödenbeck, C., Bakker, D. C. E., van Heuven, S., Hoppema, M., Metzl, N., Sweeney, C., Takahashi, T., Tilbrook, B., & Wanninkhof, R. (2015). The reinvigoration of the Southern Ocean carbon sink. *Science*, *349*(6253), 1221-1224. https://doi.org/doi:10.1126/science.aab2620

Lauvset, S. K., Lange, N., Tanhua, T., Bittig, H. C., Olsen, A., Kozyr, A., Álvarez, M., Becker, S., Brown, P. J., Carter, B. R., Cotrim da Cunha, L., Feely, R. A., van Heuven, S., Hoppema, M., Ishii, M., Jeansson, E., Jutterström, S., Jones, S. D., Karlsen, M. K.,…Key, R. M. (2021). An updated version of the global interior ocean biogeochemical data product, GLODAPv2.2021. *Earth Syst. Sci. Data*, *13*(12), 5565-5589. https://doi.org/10.5194/essd-13-5565-2021

Le Quéré, C., Rodenbeck, C., Buitenhuis, E. T., Conway, T. J., Langenfelds, R., Gomez, A., Labuschagne, C., Ramonet, M., Nakazawa, T., & Metzl, N. (2007). Saturation of the Southern Ocean CO2 sink due to recent climate change. *Science*, *316*(5832), 1735-1738.

Lenton, A., Codron, F., Bopp, L., Metzl, N., Cadule, P., Tagliabue, A., & Le Sommer, J. (2009). Stratospheric ozone depletion reduces ocean carbon uptake and enhances ocean acidification. *Geophysical Research Letters*, *36*(12).

Mackay, N., Watson, A. J., Suntharalingam, P., Chen, Z., & Landschützer, P. (2022). Improved winter data coverage of the Southern Ocean CO2 sink from extrapolation of summertime observations. *Communications Earth & Environment*, *3*(1), 265. https://doi.org/10.1038/s43247-022-00592-6

Mayot, N., Le Quéré, C., Rödenbeck, C., Bernardello, R., Bopp, L., Djeutchouang, L. M., Gehlen, M., Gregor, L., Gruber, N., & Hauck, J. (2023). Climate-driven variability of the Southern Ocean CO2 sink. *Philosophical Transactions of the Royal Society A*, *381*(2249), 20220055.

Menviel, L. C., Spence, P., Kiss, A. E., Chamberlain, M. A., Hayashida, H., England, M. H., & Waugh, D. (2023). Enhanced Southern Ocean CO2 outgassing as a result of stronger and poleward shifted southern hemispheric westerlies. *Biogeosciences*, *20*(21), 4413-4431. https://doi.org/10.5194/bg-20-4413-2023

Mignot, A., Landolfi, A., Schuckmann, K. v., Serva, F., & Landschützer, P. (2025). Sea Surface Temperature and Wind Extremes: Their Impact on Decadal Ocean Carbon Sink Variability. *ESS Open Archive*, *2025*(0829). https://doi.org/doi:10.22541/essoar.175648217.78030404/v1

Mikaloff Fletcher, S. E., Gruber, N., Jacobson, A. R., Doney, S. C., Dutkiewicz, S., Gerber, M., Follows, M., Joos, F., Lindsay, K., Menemenlis, D., Mouchet, A., Müller, S. A., & Sarmiento, J. L. (2006). Inverse estimates of anthropogenic CO2 uptake, transport, and storage by the ocean. *Global Biogeochemical Cycles*, *20*(2). https://doi.org/https://doi.org/10.1029/2005GB002530

Mongwe, P., Gregor, L., Tjiputra, J., Hauck, J., Ito, T., Danek, C., Vichi, M., Thomalla, S., & Monteiro, P. M. S. (2024). Projected poleward migration of the Southern Ocean CO2 sink region under high emissions. *Communications Earth & Environment*, *5*(1), 232. https://doi.org/10.1038/s43247-024-01382-y

Monteiro, T., Kerr, R., Orselli, I. B., & Lencina-Avila, J. M. (2020). Towards an intensified summer CO2 sink behaviour in the Southern Ocean coastal regions. *Progress in Oceanography*, 102267.

Nicholson, S.-A., Whitt, D. B., Fer, I., du Plessis, M. D., Lebéhot, A. D., Swart, S., Sutton, A. J., & Monteiro, P. M. S. (2022). Storms drive outgassing of CO2 in the subpolar Southern Ocean. *Nature Communications*, *13*(1), 158. https://doi.org/10.1038/s41467-021-27780-w

Olivier, L., & Haumann, F. A. (2025). Southern Ocean freshening stalls deep ocean CO2 release in a changing climate. *Nature Climate Change*, *15*(11), 1219-1225. https://doi.org/10.1038/s41558-025-02446-3

Olsen, A., Key, R. M., Van Heuven, S., Lauvset, S. K., Velo, A., Lin, X., Schirnick, C., Kozyr, A., Tanhua, T., & Hoppema, M. (2016). The Global Ocean Data Analysis Project version 2 (GLODAPv2)–an internally consistent data product for the world ocean. *Earth System Science Data*, *8*(2), 297-323.

Park, Y. H, Durand I. (2019). Altimetry-derived Antarctic Circumpolar Current fronts. SEANOE. https://doi.org/10.17882/59800

Park, Y. H., Park, T., Kim, T. W., Lee, S. H., Hong, C. S., Lee, J. H., Rio, M. H., Pujol, M. I., Ballarotta, M., Durand, I., & Provost, C. (2019). Observations of the Antarctic Circumpolar Current Over the Udintsev Fracture Zone, the Narrowest Choke Point in the Southern Ocean. *Journal of Geophysical Research: Oceans*, *124*(7), 4511-4528. https://doi.org/https://doi.org/10.1029/2019JC015024

Renosh, P. R., Zhang, J., Sauzède, R., & Claustre, H. (2023). Vertically Resolved Global Ocean Light Models Using Machine Learning. *Remote Sensing*, *15*(24), 5663. https://www.mdpi.com/2072-4292/15/24/5663

Roemmich, D., Alford, M. H., Claustre, H., Johnson, K., King, B., Moum, J., Oke, P., Owens, W. B., Pouliquen, S., & Purkey, S. (2019). On the future of Argo: A global, full-depth, multi-disciplinary array. *Frontiers in Marine Science*, *6*, 439.

Roobaert, A., Laruelle, G. G., Landschützer, P., Gruber, N., Chou, L., & Regnier, P. (2019). The Spatiotemporal Dynamics of the Sources and Sinks of CO2 in the Global Coastal Ocean. *Global Biogeochemical Cycles*, *33*(12), 1693-1714. https://doi.org/10.1029/2019gb006239

Rustogi, P., Landschützer, P., Brune, S., & Baehr, J. (2023). The impact of seasonality on the annual air-sea carbon flux and its interannual variability. *npj Climate and Atmospheric Science*, *6*(1), 66. https://doi.org/10.1038/s41612-023-00378-3

Sabine, C. L., Feely, R. A., Gruber, N., Key, R. M., Lee, K., Bullister, J. L., Wanninkhof, R., Wong, C. S., Wallace, D. W. R., Tilbrook, B., Millero, F. J., Peng, T.-H., Kozyr, A., Ono, T., & Rios, A. F. (2004). The Oceanic Sink for Anthropogenic CO2. *Science*, *305*(5682), 367-371. https://doi.org/10.1126/science.1097403

Sauzède, R., Bittig, H. C., Claustre, H., Pasqueron de Fommervault, O., Gattuso, J.-P., Legendre, L., & Johnson, K. S. (2017). Estimates of water-column nutrient concentrations and carbonate system parameters in the global ocean: A novel approach based on neural networks. *Frontiers in Marine Science*, *4*, 128.

Sauzède, R., Claustre, H., Uitz, J., Jamet, C., Dall'Olmo, G., D'Ortenzio, F., Gentili, B., Poteau, A., & Schmechtig, C. (2016). A neural network-based method for merging ocean color and Argo data to extend surface bio-optical properties to depth: Retrieval of the particulate backscattering coefficient. *Journal of Geophysical Research: Oceans*, *121*(4), 2552-2571. https://doi.org/https://doi.org/10.1002/2015JC011408

Siegel, D., Buesseler, K., Doney, S. C., Sailley, S., Behrenfeld, M. J., & Boyd, P. (2014). Global assessment of ocean carbon export by combining satellite observations and food-web models. *Global Biogeochemical Cycles*, *28*(3), 181-196.

Takahashi, T., Sutherland, S. C., Wanninkhof, R., Sweeney, C., Feely, R. A., Chipman, D. W., Hales, B., Friederich, G., Chavez, F., & Sabine, C. (2009). Climatological mean and decadal change in surface ocean pCO2, and net sea–air CO2 flux over the global oceans. *Deep Sea Research Part II: Topical Studies in Oceanography*, *56*(8-10), 554-577.

Takahashi, T., Sweeney, C., Hales, B., Chipman, D. W., Newberger, T., Goddard, J. G., Iannuzzi, R. A., & Sutherland, S. C. (2012). The changing carbon cycle in the Southern Ocean. *Oceanography*, *25*(3), 26-37.

Tonboe, R. and Nielsen, E. Global Sea Ice Concentration Reprocessing, Validation Report. Ocean & Sea Ice SAF, Product OSI-409, Version 1.3, September 2011.

Van Rossum, G., & Drake, F. L. (2009). Python reference manual (Vol. 111, pp. 1–52). Centrum voor Wiskunde en Informatica.

Wanninkhof, R. (1992). Relationship between wind speed and gas exchange over the ocean. *Journal of Geophysical Research: Oceans*, *97*(C5), 7373-7382. https://doi.org/10.1029/92JC00188

Wanninkhof, R. (2014). Relationship between wind speed and gas exchange over the ocean revisited. *Limnology and Oceanography: Methods*, *12*(6), 351-362. https://doi.org/10.4319/lom.2014.12.351

Watson, A. J., Schuster, U., Shutler, J. D., Holding, T., Ashton, I. G. C., Landschützer, P., Woolf, D. K., & Goddijn-Murphy, L. (2020). Revised estimates of ocean-atmosphere CO2 flux are consistent with ocean carbon inventory. *Nature Communications*, *11*(1), 4422. https://doi.org/10.1038/s41467-020-18203-3

Williams, N. L., Juranek, L. W., Feely, R. A., Johnson, K. S., Sarmiento, J. L., Talley, L. D., Dickson, A. G., Gray, A. R., Wanninkhof, R., Russell, J. L., Riser, S. C., & Takeshita, Y. (2017). Calculating surface ocean pCO2 from biogeochemical Argo floats equipped with pH: An uncertainty analysis. *Global Biogeochemical Cycles*, *31*(3), 591-604. https://doi.org/https://doi.org/10.1002/2016GB005541

Zhang, C., Wu, Y., Brown, P. J., Stappard, D., Silva, A. N., & Tyrrell, T. (2026). A systematic bias in float pH leads to overestimation of derived pCO2 and underestimation of carbon uptake by the Southern Ocean. *Scientific reports*. https://doi.org/10.1038/s41598-026-43863-4

1266 Zhang, M., Cheng, Y., Bao, Y., Zhao, C., Wang, G., Zhang, Y., Song, Z., Wu, Z., & Qiao, F. (2022).
1267 Seasonal to decadal spatiotemporal variations of the global ocean carbon sink. *Global Change*
1268 *Biology*, *28*(5), 1786-1797.
1269 Zhang, S., Chen, P., Bisson, K., Jamet, C., Di Girolamo, P., Dionisi, D., Hu, Y., Zhang, Z., Shi, K., &
1270 Pan, D. (2025). Substantially underestimated winter CO(2) sources of the Southern Ocean. *Sci*
1271 *Adv*, *11*(45), eaea0024. https://doi.org/10.1126/sciadv.aea0024